BLAST NOISE PROPAGATION PREDICTION

BY

CAROLYN RENEE SHAFFER

B.S., University of Illinois, 1987

THESIS

Submitted in partial fulfillment of the requirements
for the degree of Master of Science in Electrical Engineering
in the Graduate College of the
University of Illinois at Urbana-Champaign, 1988

Urbana, Illinois

ACKNOWLEDGEMENTS

Graduate school has been a very important part of my life because I have learned so many valuable things. Most significantly, I've come to realize that learning is life's most important task. Several people were responsible for guiding me and teaching me many different things along the way. They are acknowledged here, with affection, as follows:

Professor Rich Raspet for his support and guidance researching a subject that holds great interest for me and for allowing me to experience all that comes with research in acoustics.

Professor Steve Franke for being a knowledgeable advisor and, most important, for reminding me that, despite my failures, it's the person inside that really matters.

Professor Bill O'Brien for boosting my confidence levels when they were too low to keep trying. Without this encouragement, I may never even have applied to graduate school.

Herbert Schonken for working so diligently producing plots and for being fun to work with.

Tim Rand, Jeff Austen and Gary Stitt for word processing assistance and for keeping me motivated by checking up on my progress.

TABLE OF CONTENTS

PAGE

I. INTRODUCTION 1

II. LITERATURE SURVEY 2

III. THEORY 4

IV. PROBLEM STATEMENT 8

V. EXPERIMENTAL PROCEDURE 20

VI. DATA ANALYSIS 23

VII. RESULTS 45

VIII. CONCLUSIONS 63

REFERENCES 69

LIST OF FIGURES

PAGE

Figure 1. Spherical spreading from a point source in a neutral atmosphere. 7

Figure 2. a) Negative sound speed gradient and associated ray path diagram.
b) Positive sound speed gradient and associated ray path diagram. 7

Figure 3. Layered atmosphere with source and detector bounded by impedance surfaces. 18

Figure 4. Equivalent transmission lines for the acoustic problem of Fig. 3. 19

Figure 5. a) Site separations at Aberdeen Proving Ground, Maryland. b) Site separations at Ft. Bliss, Texas. 22

Figure 6. Nine categories of sound velocity profiles. 27

Figure 7. Sound velocity profiles for data from Ft. Bliss in the lapse category. The heavy line indicates the average curve used in the FFP. 28

Figure 8. Sound velocity profiles for data from Ft. Bliss in the constant category. The heavy line indicates the average curve used in the FFP. 29

Figure 9. Sound velocity profiles for data from Ft. Bliss in the constant below lapse category. The heavy line indicates the average curve used in the FFP. 30

Figure 10. Sound velocity profiles for data from Ft. Bliss in the low inversion category. The heavy line indicates the average curve used in the FFP. 31

Figure 11. Sound velocity profiles for data from Ft. Bliss in the medium inversion category. The heavy line indicates the average curve used in the FFP. 32

Figure 12. Sound velocity profiles for data from Ft. Bliss in the high inversion category. The heavy line indicates the average curve used in the FFP. 33

Figure 13. Sound velocity profiles for data from Ft. Bliss in the constant recurve category. The heavy line indicates the average curve used in the FFP. 34

Figure 14. Sound velocity profiles for data from Ft. Bliss in the negative recurve category. The heavy line indicates the average curve used in the FFP. 35

Figure 15. Sound velocity profiles for data from Aberdeen Proving Ground in the lapse category. The heavy line indicates the average curve used in the FFP. 36

Figure 16. Sound velocity profiles for data from Aberdeen Proving Ground in the constant category. The heavy line indicates the average curve used in the FFP. 37

Figure 17. Sound velocity profiles for data from Aberdeen Proving Ground in the constant below lapse category. The heavy line indicates the average curve used in the FFP. 38

Figure 18. Sound velocity profiles for data from Aberdeen Proving Ground in the low inversion category. The heavy line indicates the average curve used in the FFP. 39

Figure 19. Sound velocity profiles for data from Aberdeen Proving Ground in the medium inversion category. The heavy line indicates the average curve used in the FFP. 40

Figure 20. Sound velocity profiles for data from Aberdeen Proving Ground in the high inversion category. The heavy line indicates the average curve used in the FFP. 41

Figure 21. Sound velocity profiles for data from Aberdeen Proving Ground in the constant recurve category. The heavy line indicates the average curve used in the FFP. 42

Figure 22. Sound velocity profiles for data from Aberdeen Proving Ground in the positive recurve category. The heavy line indicates the average curve used in the FFP. 43

Figure 23. Sound velocity profiles for data from Aberdeen Proving Ground in the negative recurve catagory. The heavy line indicates the average curve used in the FFP. 44

Figure 24. CSEL vs. distance for lapse category data from Ft. Bliss and FFP output 46

Figure 25. CSEL vs. distance for constant category data from Ft. Bliss and FFP output 47

Figure 26. CSEL vs. distance for constant below lapse category data from Ft. Bliss and FFP output 48

Figure 27. CSEL vs. distance for low inversion category data from Ft. Bliss and FFP output 49

Figure 28. CSEL vs. distance for medium inversion category data from Ft. Bliss and FFP output 50

Figure 29. CSEL vs. distance for high inversion category data from Ft. Bliss and FFP output 51

Figure 30. CSEL vs. distance for constant recurve category data from Ft. Bliss and FFP output 52

Figure 31. CSEL vs. distance for negative recurve category data from Ft. Bliss and FFP output 53

Figure 32. CSEL vs. distance for lapse category data from Aberdeen Proving Ground and FFP output..... 54

Figure 33. CSEL vs. distance for constant category data from Aberdeen Proving Ground and FFP output. 55

Figure 34. CSEL vs. distance for constant below lapse category data from Aberdeen Proving Ground and FFP output. 56

Figure 35. CSEL vs. distance for low inversion category data from Aberdeen Proving Ground and FFP output. 57

Figure 36. CSEL vs. distance for medium inversion category data from Aberdeen Proving Ground and FFP output. 58

Figure 37. CSEL vs. distance for high inversion category data from Aberdeen Proving Ground and FFP output. 59

Figure 38. CSEL vs. distance for constant recurve category data from Aberdeen Proving Ground and FFP output. 60

Figure 39. CSEL vs. distance for positive recurve category data from Aberdeen Proving Ground and FFP output. 61

Figure 40. CSEL vs. distance for negative recurve category data from Aberdeen Proving Ground and FFP output. 62

Figure 41. Variation in CSEL vs. distance due to change in flow resistivity..... 68

I. INTRODUCTION

Many studies of sound propagation in the atmosphere have been conducted in order to predict sound pressure levels from explosives for noise abatement purposes. The development of an accurate prediction scheme would enable the producers of impulsive sounds, such as army artillery testing units, to minimize the environmental impact of the activities and to reduce community response. Researchers have observed and predicted the effects of temperature and wind gradients, turbulence and complex ground impedance on acoustic wave propagation. Several of these prediction schemes are described in Chapter II. The method of prediction at the heart of this study is a computer model referred to as the Fast Field Program (FFP). When supplied with information about sound speed variations with height and surface impedance, the FFP evaluates an approximation of the Fourier-Bessel expression for pressure over a specified propagation range. The results of the FFP are compared to blast noise levels recorded in an experiment by the U.S. Army Construction Engineering Laboratory in which meteorological data were taken simultaneously.

Detailed in Chapter III is how the FFP accounts for sound focussing and shadowing due to temperature and wind gradients. The complex ground impedance is modeled using the Delany-Bazley-Chessell model and is described in Chapter IV. Currently, effects due to turbulence are not included.

The experimental procedure is given in Chapter V, and the method of data analysis is described in Chapter VI. With an extensive data bank to study how sound velocity varied with height, classifications based on the similarity of this variation were made. Nine groups were defined in order to cover all of the observed classes. Using the grouped data allowed comparison of sound levels over a range with the prediction of the FFP. Chapter VII presents the results of the comparison. A discussion of the results follows in Chapter VIII.

II. LITERATURE SURVEY

As long ago as 1687, in the publication of Newton's Principia , it was shown that sound speed was proportional to the square root of temperature. But, it was not until the late 1800s and early 1900s that Reynolds, Whipple, Barton and Stokes, independently, discovered that temperature gradients affected sound propagation in unfamiliar ways [1]. Granted, scientists not always concerned themselves with sound pressure levels being too high; rather, they desired to devise methods which could make sound audible at large ranges. With the development of highways, airports and testing sites for military weapons, the problem became one of suppressing sound at long distances, minimizing impact and understanding the mechanisms of sound attenuation. As discussed in papers of 1953, 1954, and 1955 by Ingard, Cox et al. and Noble, respectively [2-4], predicting sound focuses and nulls due to meteorological effects were a major concern. The ability to predict when certain activities result in considerable disturbance grew critical in response to legal regulations. Subsequently, several prediction models were produced by various government agencies.

In 1964, Perkins and Jackson [5] created a handbook cataloguing eighty-seven different graphs depicting the change in sound speed with altitude and corresponding plots indicating sound ray paths. A "multiplication factor", assigned to each entry in the catalog, indicated the danger of creating public annoyance. Actual sound pressure levels were not calculated, but large amplitude explosions were implied.

In 1969, Reed [6] published a somewhat more sophisticated treatment of blast propagation. The popular ray path calculation method was among the three prediction techniques discussed. Equations governing peak amplitude as a function of such semiempirical parameters as the "focus factor" were presented.

Rasmussen [7], in 1971, tried to combine the efforts of Perkins, Jackson and Reed into one prediction method. A series of worksheets and checklists resulted which walked the user through the calculation of the component of the wind speed in the direction of the blast propagation and other mathematical manipulations which yielded the assignment of a "focus factor." This method was developed only after attempting a more rigorous computerized model by Bundgaard [8] which was

considered to require excessive computer time and atmospheric information.

About the same time, Schomer et al. [9] developed an empirically based model used in the form of a computer program that generates C-weighted day/night average sound level contours. The user supplies the computer with the source of the impulse from a list of weapons, as well as the inversion factor chosen from a table of various U.S. cities. Various army bases across the U.S. currently use this personal computer program.

Many models followed, including a recent empirical model by Kerry and Saunders [10], but none of them include complex ground impedance effects. The development of faster computers and new methods of solution for wave propagation prediction hold promise of rapid prediction of blast noise levels from the atmospheric data. To this end, calculational techniques developed for underwater acoustics were reviewed for applicability to atmospheric propagation. The Fast Field Program (FFP) predicts the sound intensity from the description of the sound speed throughout the water and the bottom characteristics. This computer model, first conceived by DiNapoli [11], and developed by Kutschale [12] and Deavenport [11], evaluated the Fourier-Bessel integral that describes pressure at an observation point due to a point source.

In 1982 , Lee et al. [13] applied this technique to atmospheric acoustics. Since the initial introduction of the FFP to the atmosphere, some changes have occurred. Originally the spectrum that must be calculated to evaluate the Fourier-Bessel integral was computed by using propagation matrix techniques. This method proved to be numerically unstable and produced unreliable results [13]. The current version is discussed in Chapter IV. A comparison between the old version and the current one can be found in [14].

III. THEORY

Atmospheric effects play an enormous role in the redirection of sound energy so that it is focussed in some places and absent in others. This is known as atmospheric refraction and results from spatial variations in sound speed.

As a starting point, it is convenient to look at spherical spreading from a point source in a homogeneous atmosphere. That is, an atmosphere that has constant sound speed everywhere. The wave equation for spherically symmetric pressure fields is

$$\frac{\partial^2 p}{\partial r^2} + \frac{2}{r}\frac{\partial p}{\partial r} = \frac{1}{c^2}\frac{\partial^2 p}{\partial t^2}$$

where p is pressure, r is radial distance and c is the sound speed. If we rewrite the above equation with rp as the dependent variable, we obtain an equation of the same form as the plane wave equation, as shown:

$$\frac{\partial^2 (rp)}{\partial r^2} = \frac{1}{c^2}\frac{\partial^2 (rp)}{\partial t^2}$$

The general solution of this equation for an impulsive source for pressure as a function of time and space is

$$p = \frac{1}{r} f\left(t - \frac{r}{c}\right)$$

where f(t - r/c) determines when the pulse, beginning at some time, t, will reach an arbitrary point. The amplitude factor, 1/r, accounts for the decrease in sound intensity with distance. Given spherical symmetry and a neutral atmosphere, the sound energy flows radially from the source as shown in Figure 1. All figures appear at the end of the chapter.

Note that in Figure 1 the arrows indicated as radiating from the source are known as sound rays. As in geometrical optics, they represent the direction of travel of a wave front. A wave front is merely an outwardly radiating spherical surface of constant phase.

It is now appropriate to introduce the concept of ray tracing. A thorough discussion of ray acoustics appears in texts by Pierce and Lindsay [15-16].

As evidenced in the above configuration, the rays emanating from the source showed no

preference towards a particular direction of propagation, since the sound speed is constant in all directions. Another unrealistic but technically correct situation where this would occur is if the sound speed varied with spherical symmetry about the source.

In practice, what we really have is sound speed that varies with height such that we can regard the atmosphere as consisting of many layers, each of constant sound speed. Ray tracing helps us to look at this problem by indicating where sound is refracted.

Commonly, we see temperature decreasing with increasing altitude. This indicates a decreasing sound velocity with height as well. A subsequent bending of rays towards the lower sound speed occurs, and thus we have upward refraction. A greater than normal attenuation of sound in the lateral direction results in this situation, and we obtain an effect known as a shadow zone. According to the geometrical acoustics approximation, no sound will propagate into the shadow zone.

Temperature increasing with height also occurs such that rays bend toward the ground toward lower sound speeds. This creates an increase in sound levels. Figure 2 shows these two cases and a corresponding graph of sound speed gradient vs. height.

These two examples make clear how strongly dependent sound propagation is on meteorological conditions. This is due to sound speed being dependent on temperature and on the wind direction and speed. A brief discussion of how the atmosphere usually changes from day to night follows.

The ground plays an important role when considering diurnal temperature variations. During daylight, the earth acts as an absorber of the sun's energy and conducts heat to the layer of air near the surface. A sound speed gradient as in Figure 2 a) is produced. Alternately, the earth's outgoing radiation exceeds its incoming at nighttime. The ground loses the heat that it gained from the sun during the day and cools. As the surface cools, the air layer near the ground also cools such that temperatures actually increase with height before they eventually start decreasing. This is known as a temperature inversion and can sometimes be visible as fog, since air is trapped, cooled and condensed in the lower atmosphere.

This process repeats itself when the sun reappears and reheats the ground which again raises

temperatures in the lowest air layer. The heated air pushes the inversion layer higher throughout the day and finally dissipates from wind and sun influences. Geiger's text [17] offers a more rigorous presentation of climatic changes.

The problem is now reduced to one of predicting sound levels given atmospheric conditions and terrain information. The formal problem statement follows in the next chapter.

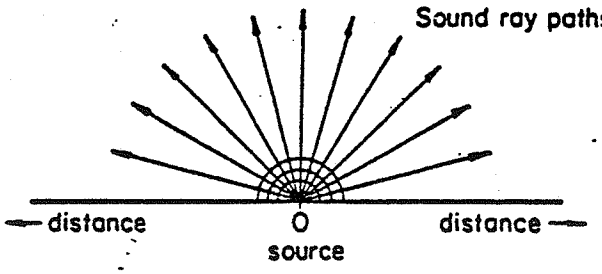

Figure 1. Spherical spreading from a point source in a neutral atmosphere.

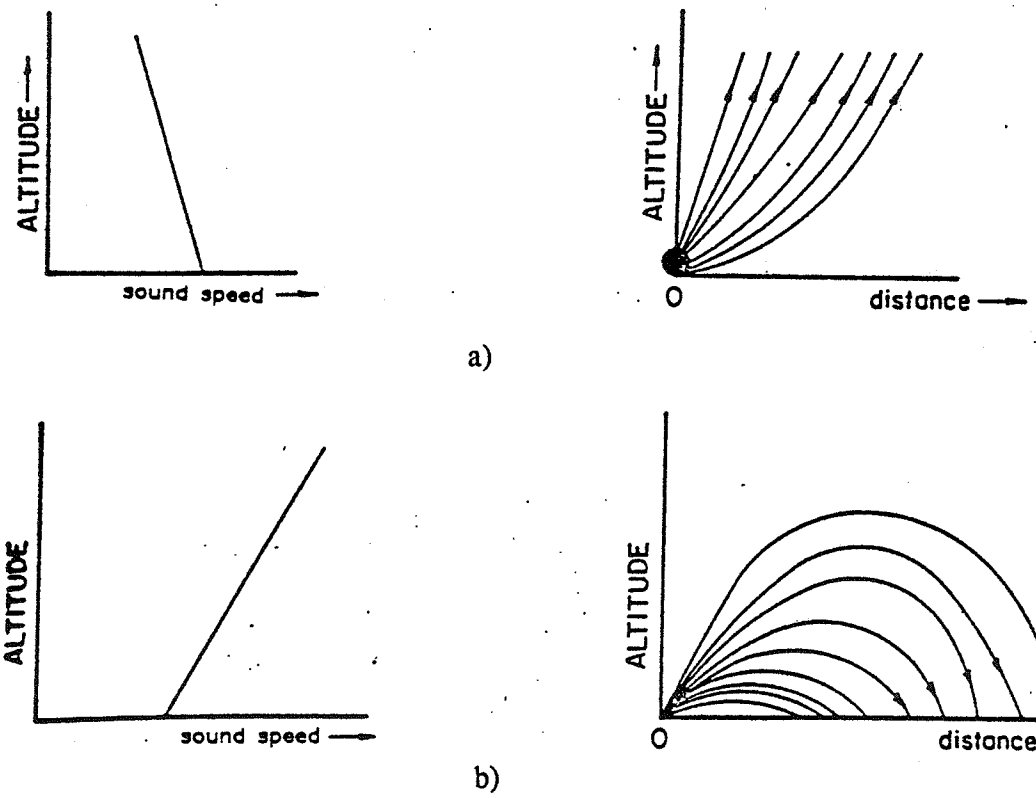

Figure 2. a) Negative sound speed gradient and associated ray path diagram. b) Positive sound speed gradient and associated ray path diagram.

IV. PROBLEM STATEMENT

The general statement of this problem is most easily made pictorially. Figure 3 shows the atmosphere as consisting of (n-1) layers. An impulsive point source is located at the bottom of layer S at r=0 and $z=z_S$ in cylindrical coordinates. The detector is located at the bottom of layer D at r=r and $z=z_D$. We would like to to locate the receiver arbitrarily and determine the pressure at that point. As one might imagine the applications of such an accurate prediction are numerous.

Two impedance boundary conditions must be enforced at z=0 and $z=z_{n-1}$. Reference [13] gives these expressions and are repeated here for convenience.

At a surface z=a, the surface impedance is defined by the pressure, p, and the vertical particle velocity, u. In the transform domain, where k is the transform variable and can be thought of as the horizontal wave number, the surface impedance is

$$Z(k) = \text{sgn}\ \frac{p\,(k, z=a)}{u\,(k,z=a)}$$

where

sgn = +1 if u moves into the impedance surface

or sgn = -1 if u moves away from the surface

For our problem, sgn=-1 for a=0, the top impedance, Z_t, and sgn=+1 for $a=z_{n-1}$, the bottom impedance, Z_b. Above the defined (n-1) layers a liquid half space is assumed such that,

$$Z_t = \frac{\omega\rho_o}{\sqrt{k_o - k^2}}$$

where for m=0,1,2,...,n :

ρ_m=density of layer m in kg/m^3

c_m=acoustic wave speed in layer m in m/s

$k_m=\omega/c_m$=wavenumber in layer m in m^{-1}.

The bottom surface is described empirically by the Delany-Bazley-Chessell model [18-19] as

$$Z_b(k) = \frac{R + iX}{\sqrt{1 - (\frac{k}{k_{c_n}})^2}}$$

where

$$R = (\rho_n c_n)\left[1 - 9.08 \left(\frac{f}{\sigma}\right)^{-0.75} \right]$$

$$X = -(\rho_n c_n)\ 11.9 \left(\frac{f}{\sigma}\right)^{-0.73}$$

σ=specific flow resistance per unit thickness in $g/s/cm^3$

$f=\omega/2\pi$ in Hz.

Starting with the Helmholtz equation for acoustic pressure,

$$\nabla^2 p(x,y,z) + k^2 p(x,y,z) = -4\pi\,\delta(x)\delta(y)\delta(z - z_s)$$

where $k^2 = k^2(z) = \omega^2/ c^2(z)$.

Since the medium is cylindrically symmetric we can write the Helmholtz equation in cylindrical coordinates eliminating angle dependence:

$$\frac{\partial^2 p}{\partial r^2} + \frac{1}{r}\frac{\partial p}{\partial r} + \frac{\partial^2 p}{\partial z^2} + k^2 p = -\frac{2}{r}\,\delta(r)\delta(z - z_s)$$

In two-dimensional systems with circular symmetry, the two independent variables may be

reduced to one radial variable. The appropriate expression is the Hankel transform. This is a one-dimensional transform with a Bessel kernel, where the pair is defined as

$$p(r,z) = \int_0^\infty P(k,z)\, J_o(kr)\, k\, dk$$

$$P(k,z) = \int_0^\infty p(r,z)\, J_o(kr)\, r\, dr$$

and P is the Hankel transform of the pressure and k is the transform variable. The variable k can be thought of as the horizontal wavenumber.

The Helmholtz equation in terms of the Hankel transform is

$$\frac{d^2P}{dz^2} + (k^2(z) - K^2)\, P = -\frac{2p_o}{i\rho_o\omega}\, \delta(z - z_s)$$

Our main goal now is to solve for P and use it to solve for the integral expression for p(r,z) as stated above in the inverse Hankel transform. To simplify this task, the previous equation can be written, equivalently, as

$$\frac{dP}{dz} = -i\, \omega\rho_o\, U_z$$

$$\frac{dU_z}{dz} = -i\frac{k^2(z) - K^2}{\omega\rho_o}\, P + \frac{2\, p_o}{i\, \omega\rho_o}\, \delta(z - z_s)$$

where U_z is the vertical component of the transformed particle velocity, ρ_O is the unperturbed fluid density and p_O is the ambient pressure. The delta function in the second equation indicates that a constant pressure source produces a discontinuity of $2p_O/i\omega\rho_o$ in the vertical velocity.

The similarity between these equations and the Telegrapher's equations for a nonuniform

transmission line with a source emerges. The Telegrapher's equations are shown here for clarity.

$$\frac{\partial}{\partial z} V_m(z) = -Z_m I_m(z)$$

$$\frac{\partial}{\partial z} I_m(z) = -Y_m V_m(z) + I_o \delta(z - z_s)$$

The variable V_m is the voltage, I_m is the current, Z_m is the distributed series impedance per unit length in ohms/m and Y_m is the distributed shunt impedance per unit length in S/m, and I_o is the amplitude of the current source. It is obvious that there exists a one-to-one correspondence between P and voltage and between U_z and current. In fact, when solving by this method $P(k,z_D)$ equals $V_m(z_D)$ and defines the spectrum of the pulse at z_D, F(k). Table 1 of [14] details the other analogies for propagation constants and characteristic impedances.

The calculation of F(k) is deferred momentarily to simplify the above inverse Hankel integral equation. We can rewrite the Bessel function in terms of Hankel functions.

$$J_0(kr) = 1/2\,[H_0^{(1)}(kr) + H_0^{(2)}(kr)]$$

The incoming wave factor, $H_0^{(1)}(kr)$, is negligible and the Bessel function can be replaced by the outgoing wave alone [11].

The second-order Hankel function allows approximation in the far field as

$$H_o^{(2)}(kr) = \sqrt{\frac{2}{kr\pi}}\, e^{-i\left(kr - \frac{\pi}{4}\right)}$$

Finally, we have

$$T(\omega, r) = \frac{p(r)}{p_o} = \frac{e^{i\frac{\pi}{4}}}{\sqrt{2\pi r}} \int_0^{k_{max}} P(k, z_D)\, e^{-ikr} \sqrt{k}\, dk$$

where the upper limit of integration has been truncated at the maximum horizontal wave number.

Before approximating the integral as a summation, one should note our assumption of lossless layers. If even one of the layers is lossy, we must consider it by generalizing the wave number for each layer, m, as

$$k_m^2 = \left(\frac{\omega}{c_m}\right)^2 \left[1 - i\left(\frac{2\alpha_m c_m}{\omega}\right) \right]$$

where α_m is the attenuation coefficient.

In a lossless medium, certain values of k, corresponding to surface waves supported by the layered structure, lead to an infinite spectrum, F(k). To avoid numerical difficulties, a very small artificial loss was added and later removed from the final solution.

We may now write the integral indicated above as a summation to be evaluated by the Fast Fourier Transform.

$$T(\omega, r_m) = \frac{p(r_m)}{p_o} = \Delta k \sum_{n=0}^{N-1} P(k_n) \sqrt{k_n}\, e^{-inr_o\Delta k}\, e^{-i2\pi nm/N}$$

for n=0,1,2,...,N-1

where

$\Delta k = k_{max} / (N - 1)$ is the increment in wavenumber,

$\Delta r = 2\pi / N(\Delta k)$ is the increment in range

$k_n = n(\Delta k)$ for n=0,1,2,...,N-1 is the wavenumber in layer m

$r_m = r_o + m(\Delta r)$ for m=1,2,3,...,N is the nth range calculated

r_o = starting range point

N = steps of integration.

Of note here is that the FFT used is accomplished by the overlap and add technique on a Cyber 175 where there are 1024 points per panel. An important consideration is to meet or exceed the Nyquist rate by choosing the correct number of panels. That is,

$$\text{number of panels} = (r_{max}\, k_{max}) / 1024\, \pi$$

This insures adequate sampling of the exponential term but not necessarily the $P(k)\, k^{1/2}$ term. Continuing towards a solution, we note that from system theory we know the Fourier Transform of the input pulse at an arbitrary distance, r, is equal to the transfer function of the medium multiplied by the Fourier Transform of the input pulse at the origin, $\tilde{P}(\omega,0)$. Let $G(\omega,r)$ be the Fourier Transform of the input pulse at r.

$$G(\omega,r) = T(\omega,r)\, \tilde{P}(\omega,0)$$

Transforming back to the time domain using the inverse Fourier integral, we get

$$g(t) = \frac{1}{2\pi} \int_{-\infty}^{+\infty} T(\omega,r)\, \tilde{P}(\omega,0)\, e^{i\omega t}\, d\omega$$

Essential for calculation of sound exposure levels (SEL) is the integral of the square of g(t). This is obtained using Parseval's Relation.

$$\int_{-\infty}^{+\infty} g^2(t)\, dt = \frac{1}{\pi} \int_{0}^{\infty} |T(\omega,r)|^2\, |\tilde{P}(\omega,r)|^2\, d\omega$$

This can then be evaluated as a summation,

$$\int_{-\infty}^{+\infty} g^2(t)\,dt = \frac{\Delta\omega}{\pi} \sum_{n=0}^{N} |T(\omega_n)|^2 |\tilde{P}(\omega_n)|^2$$

It should be noted that by taking the integral of the square of g(t), fewer points are necessary for sampling as shown by Franke [20]. Upon squaring, we consider only the magnitude and not the phase. This is a substantial savings in computer time. Finally, we have used the above calculation in computing the SELs. They are

$$\text{F-SEL} = 10 \log \frac{\int g^2(t)\,dt}{(20 \times 10^{-6})^2}$$

$$\text{C-SEL} = 10 \log \frac{\int g_c(t)\,dt}{(20 \times 10^{-6})^2}$$

where F-SEL is the flat-weighted SEL, C-SEL is the C-weighted SEL and $g_C(t)$ is the C-weighted pulse shape. The reference pressure is atmospheric pressure and has the value of 20×10^{-6} Pascal.

C-weighting is equivalent to a bandpass filter with double poles at 20 Hz and 20 KHz, respectively. It is used for high amplitude sound and for response of structures to blast noise.

One should note the usage of SELs as opposed to peak levels. Prior blast studies commonly used peak levels. However, we used SELs, as the CSEL is the ANSI standard as well as the Department of Defense standard for environmental assessment and human response studies.

Now that the path to the solution has been established, we return to the discussion of how F(k), the spectrum, is obtained.

To start, the layers shown in Figure 3 are replaced by segments of transmission line as shown in Figure 4. This is now a problem of transmission lines in cascade. The voltage and current in each section, m, are governed by the Telegrapher's equations that appeared earlier in this chapter. The

attenuation constant and characteristic admittance are, respectively;

$$\gamma_m = \sqrt{Z_m Y_m}$$

$$Y_{c_m} = \sqrt{\frac{Y_m}{Z_m}}$$

It should now be noted that the voltage at the detector is exactly equal to the desired spectrum, F(k). That is,

$$F(k) = V(z_D) = P(k, z_D)$$

The computer algorithm calculates and saves the attenuation constant for each layer above the source to the detector. An important consideration is to determine when the contribution for a particular k at the source is negligible. The attenuation parameter, A, is defined as

$$A = T_m \, Re(\gamma_m)$$

where T_m is the thickness of layer m. This is compared to a predetermined value, exp $(-A_{max})$, such that if it is greater, then no further computations are deemed necessary for this particular k. The value of $\exp(-A_{max})$ is usually set equal to 10^{-6}. Otherwise, the attenuation constant is calculated for the next layer such that the attenuation parameter is now

$$A = T_m \, Re(\gamma_m) + T_{m-1} \, Re(\gamma_{m-1})$$

This value is now compared to A_{max}. If the value is smaller than A_{max}, the procedure continues until reaching the receiver.

If $A_{max} > A$ in the transmission line segments beyond the detector, a new comparison is made. A is then compared with 1/2 A_{max} . If A is greater than 1/2 A_{max}, the current section of transmission line is replaced by its characteristic admittance and ignores the rest of the transmission line cascade. If A is less than 1/2 A_{max}, the process continues as previously described. The same

procedure is followed for those layers below the source.

Finally, we can determine the voltage at the source by using

$$\frac{Y_{n-1}}{Y_{c_{n-1}}} = \frac{1 + \frac{Y_n}{Y_{c_n}} \tanh(\gamma_n T_n)}{\left(\frac{Y_n}{Y_{c_n}}\right) + \tanh(\gamma_n T_n)}$$

where n is the number of transmission line segments between the source and the final segment that was replaced by its characteristic admittance. This is used to find Y_{O+} at z=0+ and Y_{O-} at z=0-. The voltage at the source is expressed as

$$V_O = I_O / (Y_{O+} + Y_{O-})$$

Now, the voltage at the detector (the spectrum) is found by first assuming some value for it, such as unity. Then, moving backwards towards the source, we calculate the voltage for each segment, using

$$\frac{V_{n-1}}{V_n} = \frac{1 + R_n e^{-2\gamma_n T_n}}{(1 + R_n) e^{\gamma_n T_n}}$$

where R_n is the reflection coefficient at $z=z_n$. R_n is defined as

$$R_n = \frac{1 - \frac{Y_n}{Y_{c_n}}}{1 + \frac{Y_n}{Y_{c_n}}}$$

We can now obtain a value for the source voltage. The real value of the detector voltage is then

determined by proportionality as

$$\frac{\text{detector voltage}}{\text{assigned detector voltage}} = \frac{\text{source voltage}}{\text{calculated source voltage}}$$

Finally, the spectrum is obtained and the pressure at an arbitrary distance from the source can be calculated using the equation for $T(\omega,r_m)$ that appeared earlier in this chapter.

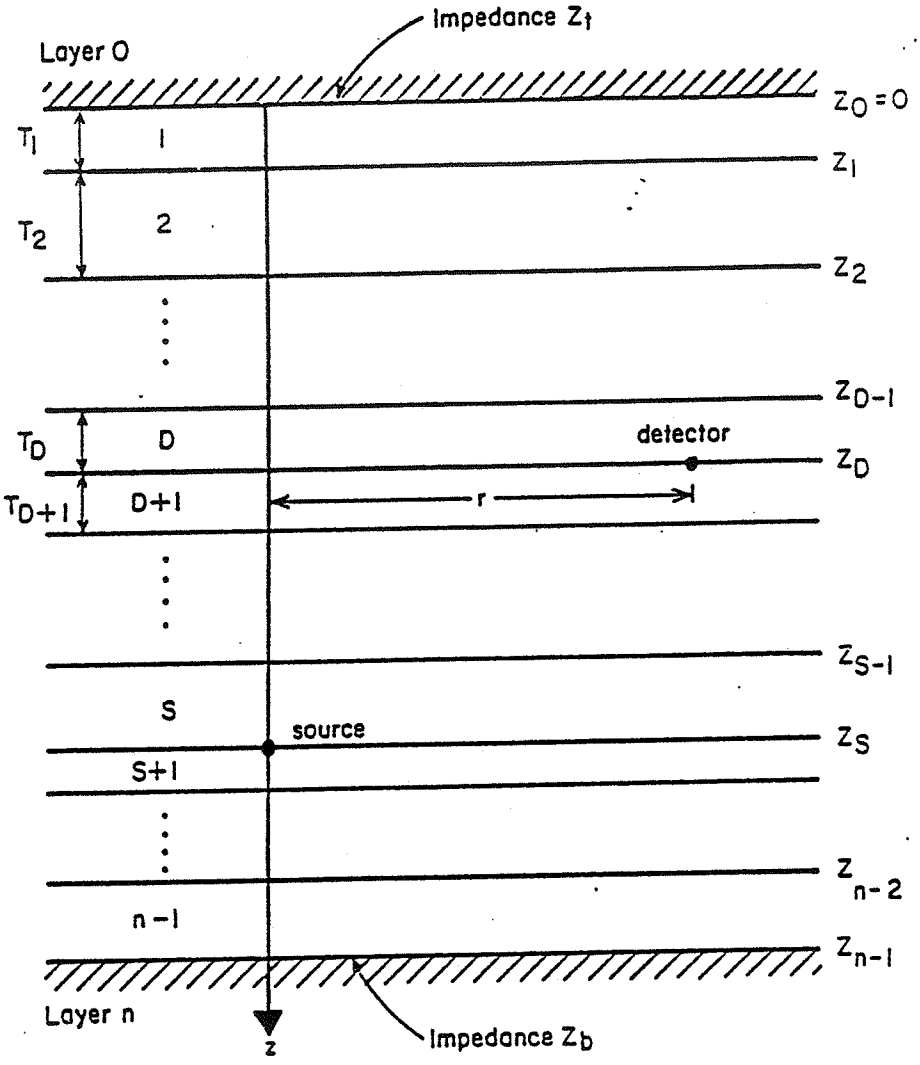

Figure 3. Layered atmosphere with source and detector bounded by impedance surfaces.

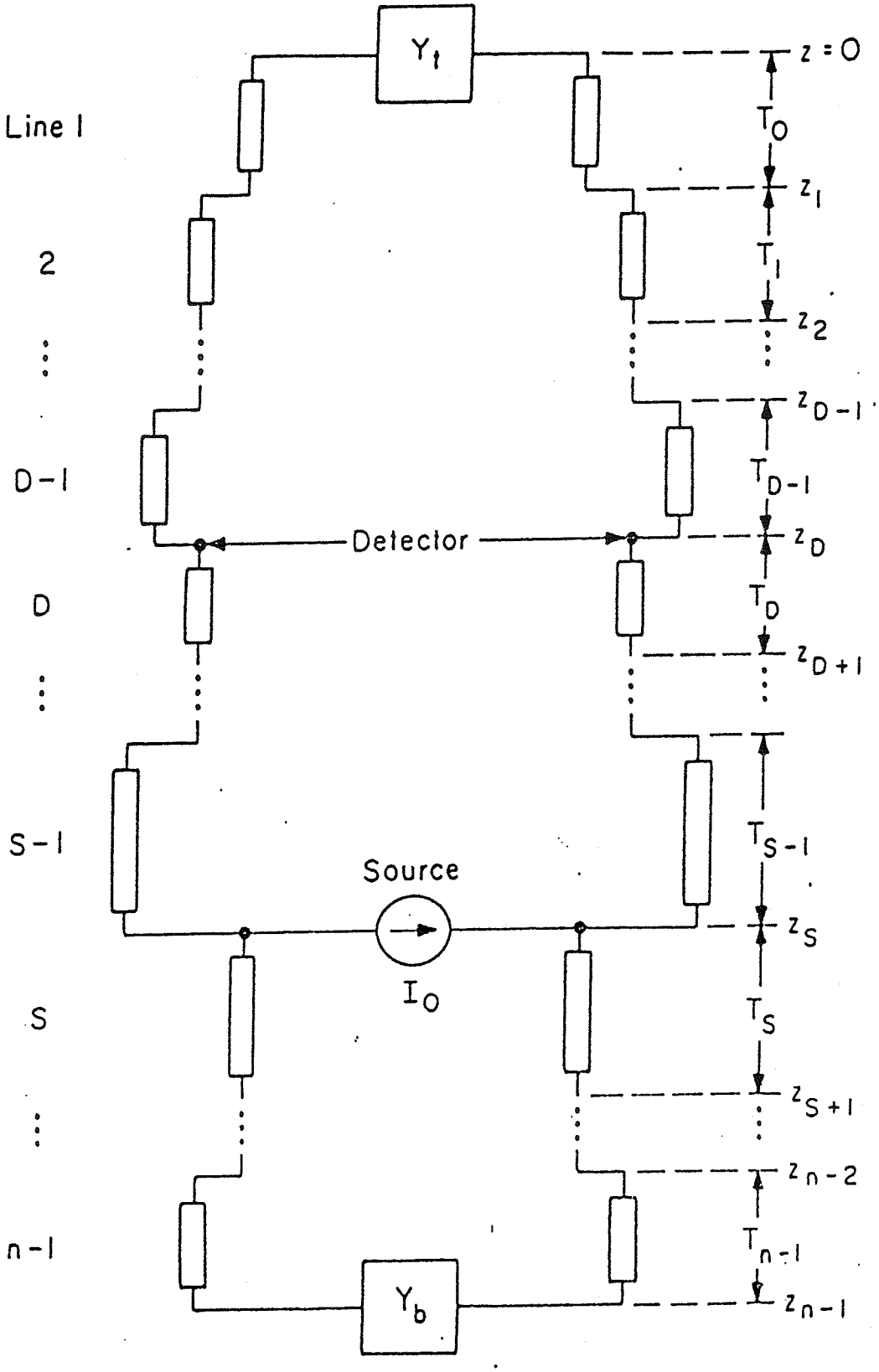

Figure 4. Equivalent transmission lines for the acoustic problem of Fig. 3.

V. EXPERIMENTAL PROCEDURE

Making an evaluation of the accuracy of the FFP's prediction required experimental data consisting of SEL versus range. The U.S. Army Corps of Engineers Construction Engineering Research Laboratory (CERL) in a combined effort with the Combat Systems Test Activity and the USAF 6th Weather Squadron of Scott AFB performed simultaneous acoustic and meteorological measurements at two locations. The first experiment was conducted at Fort Bliss, Texas over sandy, hilly terrain in June 1983. The brush-covered hills were roughly hemispherical with a radius of approximately four meters and a height of about two meters and spaced arbitrarily. The second set of measurements was taken in June 1984 at Aberdeen Proving Ground, Maryland, and was entirely over water.

The setup of the two experiments differed slightly in each case, yet were similar in most aspects. In both cases, the source was positioned on a post approximately one meter high in order to avoid direct explosion interaction with the surface. At each experiment location, explosions alternated between two sites such that measurements were taken between the two blast sites, first in one direction and then back.

The blasts originated from the ignition of C-4 plastic explosives. Blast sizes alternated between one and a quarter pounds and five pounds of plastic explosives. It is estimated that the impulsive nature of a blast of five pounds of plastic explosives is similar in duration and magnitude to the blast noise and projectile noise of a large gun.

Fort Bliss blast data were taken over sixteen kilometers, while Aberdeen Proving Ground data were taken over about twenty-six kilometers. There were eight measurement sites between blast sites at Fort Bliss and nine at Aberdeen Proving Ground. Figure 5 shows the spacing of these sites. The spacing is deliberately tighter near the source for good resolution.

At each measurement location a technician recorded peak, flat- and C-weighted sound exposure levels. The measurement system was composed of a Brüel and Kjaer model 4921 outdoor microphone, a CERL model 370 True-Integrating Environmental Noise Monitor and Sound Exposure

Level Meter and a Nagra tape recorder. The CERL noise monitor has two channels such that one is assigned to C-weighted SEL and the other to flat-weighted SEL. A separate device in parallel, with one of the two channels recorded the peak SEL. Reference [21] offers more information on the circuitry and operation of the CERL noise monitor/SEL meter. The CERL noise monitor also turned the tape recorder on and off corresponding to the beginning and end of the sample period.

Meteorological data were gathered at the midpoint between the two blast sites. Both a tethersonde and freesondes recorded the wind speed, wind direction, pressure, temperature and relative humidity versus altitude. A CERL employee operated the Atmospheric Instrumentation Research, Inc. model TS-IBR-X tethered balloon. From the electronic unit onboard, the height is indicated by a pressure change sensor. The temperature obtained by use of precision matched thermistors is measured to an accuracy of $\pm$ 0.5 ° C. The pressure change with height sensed by a temperature-compensated aneroid transducer is accurate to $\pm$ .25 m/s while wind direction is accurate to $\pm$ 5 °. The plan to run the tethersonde up three or four times per hour was rarely achieved due to difficulty and wind. The height to which the tethersonde was flown was also determined by the wind conditions. In most cases, data were obtained to about three hundred meters. The sampling of weather data began approximately fifteen minutes before sound-level measurements began and continued until about fifteen minutes afterward. Typically the tethersonde was flown up and down two or three times during this time period. USAF 6th Weather Squadron of Scott AFB operated the GMD-1 freesondes by releasing them at the midpoint at both the Aberdeen Proving Ground and Ft. Bliss site arrays. Data were taken to five thousand meters in one hundred meter increments.

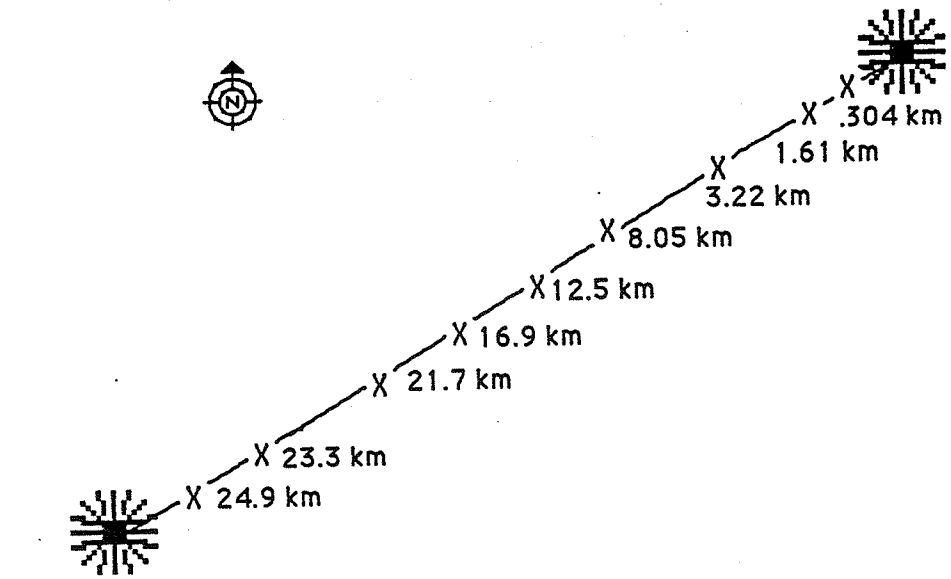

a)

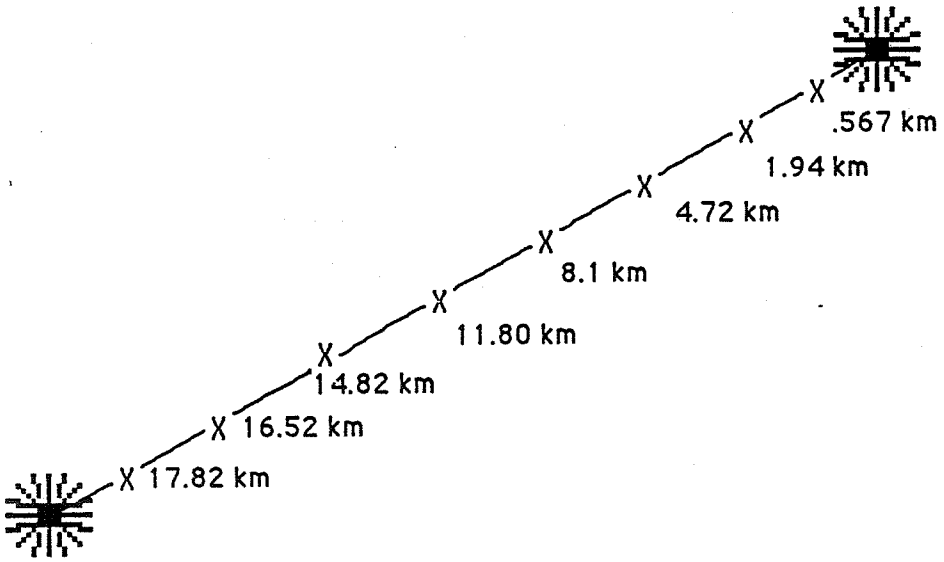

b)

Figure 5. a) Site separations at Aberdeen Proving Ground, Maryland. b) Site separations at Ft. Bliss, Texas.

VI. DATA ANALYSIS

The meteorological data taken allowed for the calculation of sound speed for each height at which readings were made. Knowing how the sound speed varies with altitude yields what will be referred to as a sound velocity profile. In order to obtain a sound velocity profile, first the temperature information at each height is used in the Goff-Gratch equation [22] to solve for the partial pressure of saturated water vapor, p_{sat}, at temperature, T. This empirical equation relates p_{sat} to T as

$$\log_{10}(p_{sat}/p_o) = 10.79586[\,1 - (T_{01}/T) - 5.02808\,\log_{10}(T/T_{01}) +$$
$$1.50474\times10^{-4}(\,1 - 10^{-8.29692[(T/T_{01}) - 1]}\,) +$$
$$0.42873\times10^{-3}(10^{4.76955[\,1 - (T_{01}/T)]} - 1\,) -$$
$$2.2195983$$

where $T_{01} = 273.16$ K and p_o is the reference pressure with value 1.013×10^5 Pascal.

Upon arriving at a solution for p_{sat}, the fraction of water molecules in air, h, can be calculated using the following relationship:

$$h = \frac{10^{-2}\,(RH)\,p_{sat}}{p}$$

where RH is the relative humidity in percent and p is the pressure. Both quantities are obtained experimentally.

Finally, assuming adiabatic wave propagation for an ideal gas, the sound speed, c, is equal to $(\gamma RT)^{1/2}$, where γ is the ratio of specific heats and R is the universal gas constant. The presence of water molecules alters the sound speed by lowering g and increasing R. The rise in R dominates so that the overall effect of increasing humidity is an increasing sound speed. These changes can be

quantified as follows:

$$\gamma = \frac{7+h}{5+h}$$

$$R = \frac{R_o}{29 - 11h}$$

where R_O = 8314.16 J/(kg K).

In this calculation of sound speed, wind speed has not yet been taken into account. This is done as follows:

$$c_{adj} = c + w \cos(\theta_w - \theta_p)$$

where c_{adj} is the adjusted sound speed, w is the wind speed, θ_w is the angle of wind propagation from north taken as zero degrees and θ_p is the angle of sound propagation also from zero degrees at north. As one would expect, the sound speed increases when a component of the wind is in the same direction as the sound propagation and decreases when in opposition.

Several conditions must be assumed in treating wind speed as an additive component to sound speed. As indicated in [15], it is assumed that the wind velocity field varies negligibly along the direction of sound propagation. Also, the normal to the wavefront is taken to be parallel with the wind velocity. It is assumed that the rays are either nearly horizontal and in one vertical plane or that the drift into the third dimension, caused by crosswinds, is negligible or averaged to be roughly zero. This allows for a two-dimensional ray trace and a treatment of the adjusted sound speed to be as the ray's velocity plus the wind velocity.

A program entitled proflu, developed by the staff of the acoustics team at CERL, calculates the sound speeds at each height for each blast and generates corresponding plots. After all plots are produced it is possible to compare sound velocity profiles and group the similar ones together. In the lower region where both tethersonde and freesonde data are available, the points roughly at the center of the distribution determine the sound velocity profile category. Nine categories were chosen to

represent all of the data acquired. The nine groups are

1. Constant
2. Lapse
3. Lapse Above Constant
4. Low Inversion
5. Medium Inversion
6. High Inversion
7. Constant Recurve
8. Negative Recurve
9. Positive Recurve

The terminology selected describes the way the sound speed varies with height. For clarification, a lapse is a linearly decreasing profile with height. Constant is an atmosphere with a uniform sound speed at all heights. Lapse above constant merely denotes a constant profile in the lower atmosphere that culminates in a lapse at higher altitudes. The inversions all have increasing sound velocity up to some point and then turn back to decreasing sound velocities. The height of the maximum sound velocity distinguishes the three types of inversions. Low inversions have a maximum around 100 meters, medium inversions at about 200 to 300 meters, and high inversions at around 400 to 500 meters.

The recurves are not quite as obvious and require some description. First, the negative recurve starts with a sound speed higher at the ground and decreases with height until it curves back to higher speeds again. The higher speeds do not exceed those at the ground. The profile then decreases again. Second, the positive recurve is the same except that when the speeds start to increase they do exceed those at the ground before they start decreasing again. The constant recurve is just a constant profile that jumps to another constant at some height. Figure 6 shows these nine categories.

The grouping of the experimental data is broken down as shown.

Ft. Bliss: 58 blasts recorded

10 constants	2 medium inversions	0 positive recurves
12 lapses	7 high inversions	3 negative recurves
13 low inversions	7 constant below lapse	4 constant recurves

Aberdeen Proving Ground: 58 blasts recorded

2 neutrals	7 medium inversions	4 positive recurves
9 lapses	10 high inversions	10 negative recurves
11 low inversions	4 neutral below lapse	1 neutral recurve

Using the Lotus Development Corporation's 1-2-3 software package, each individual sound velocity profile was plotted corresponding to its category. These plots are shown in Figures 7-23 with a heavy line through the center of the distribution of curves indicating the estimated average. These figures appear at the end of Chapter VI. The average curves were then used as a typical profile from each category for use in the FFP for comparison with the actual data.

Several things should be noted here. First, the grouping of the profiles appears much tighter in the Ft. Bliss sound velocity profiles than the Aberdeen Proving Ground ones. This is a superficial difference due to the fact that the Aberdeen plots were drawn first and graphical techniques improved with time. It should be noted that the absolute sound velocity is not important, but it is the change in sound velocity with height that produces refraction. The actual data may or may not be shifted by a constant in order to display the similarity of the curves. Second, in all cases the typical profile used in the FFP extended up to 100 meters only. The reason for this is discussed in Chapter VIII. Twelve layers were used with the bottom two layers being one meter thick, the third layer eight meters thick and the remaining nine layers ten meters each. Twelve layers proved to be sufficient for convergence, since using twenty layers gave the same result.

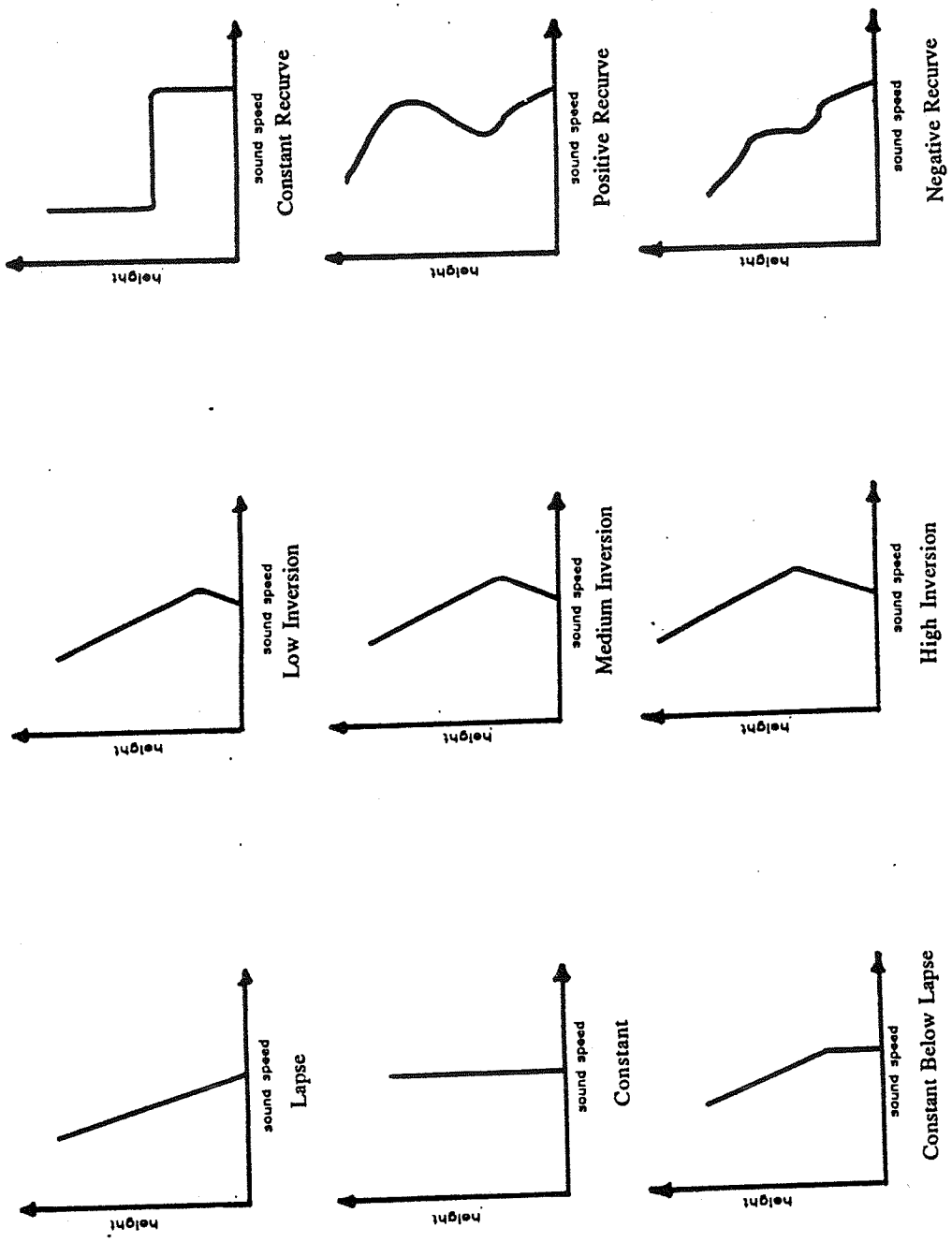

Figure 6. Nine categories of sound velocity profiles.

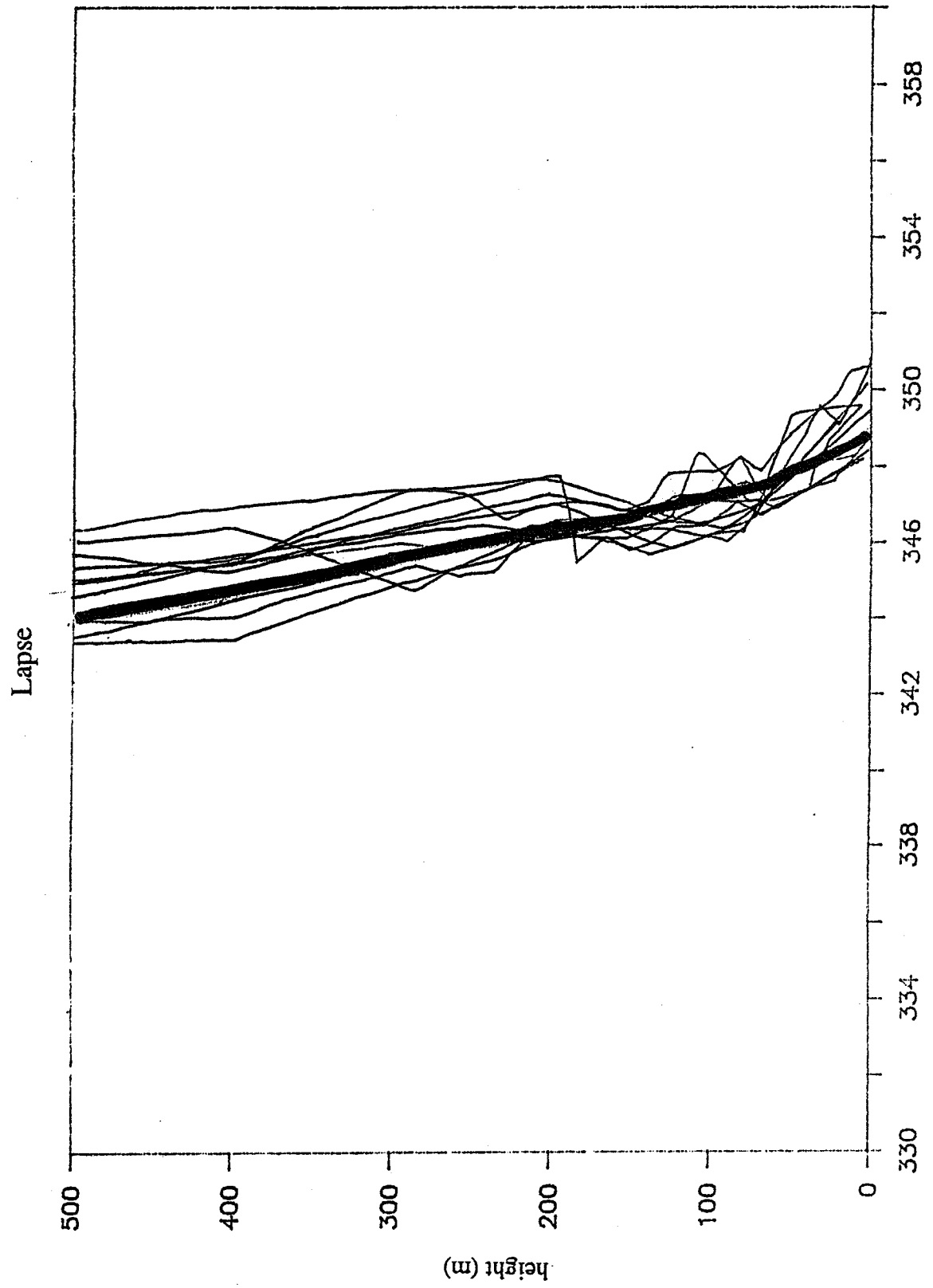

Figure 7. Sound velocity profiles for data from Ft. Bliss in the lapse category. The heavy line indicates the average curve used in the FFP.

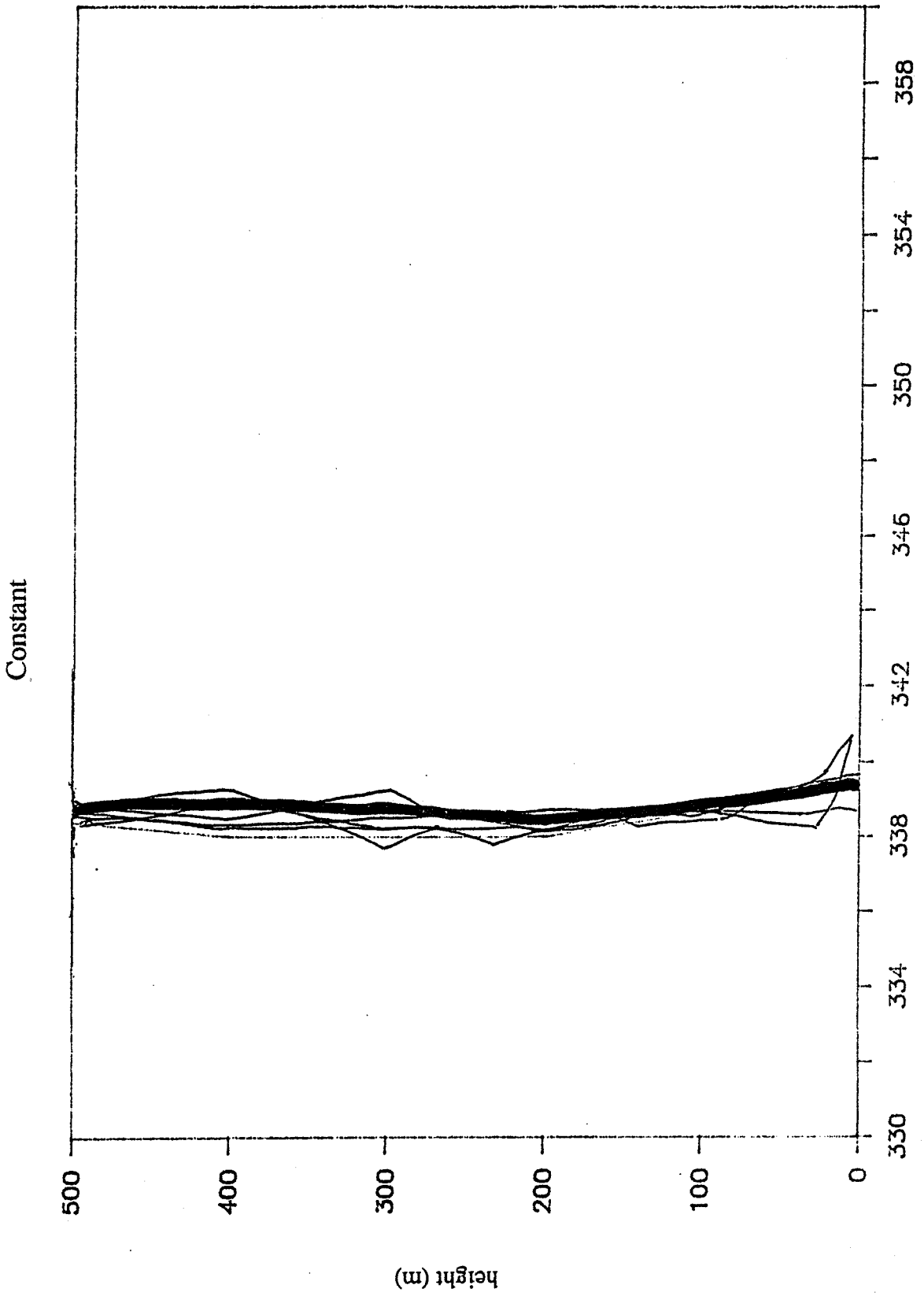

Figure 8. Sound velocity profiles for data from Ft. Bliss in the constant category. The heavy line indicates the average curve used in the FFP.

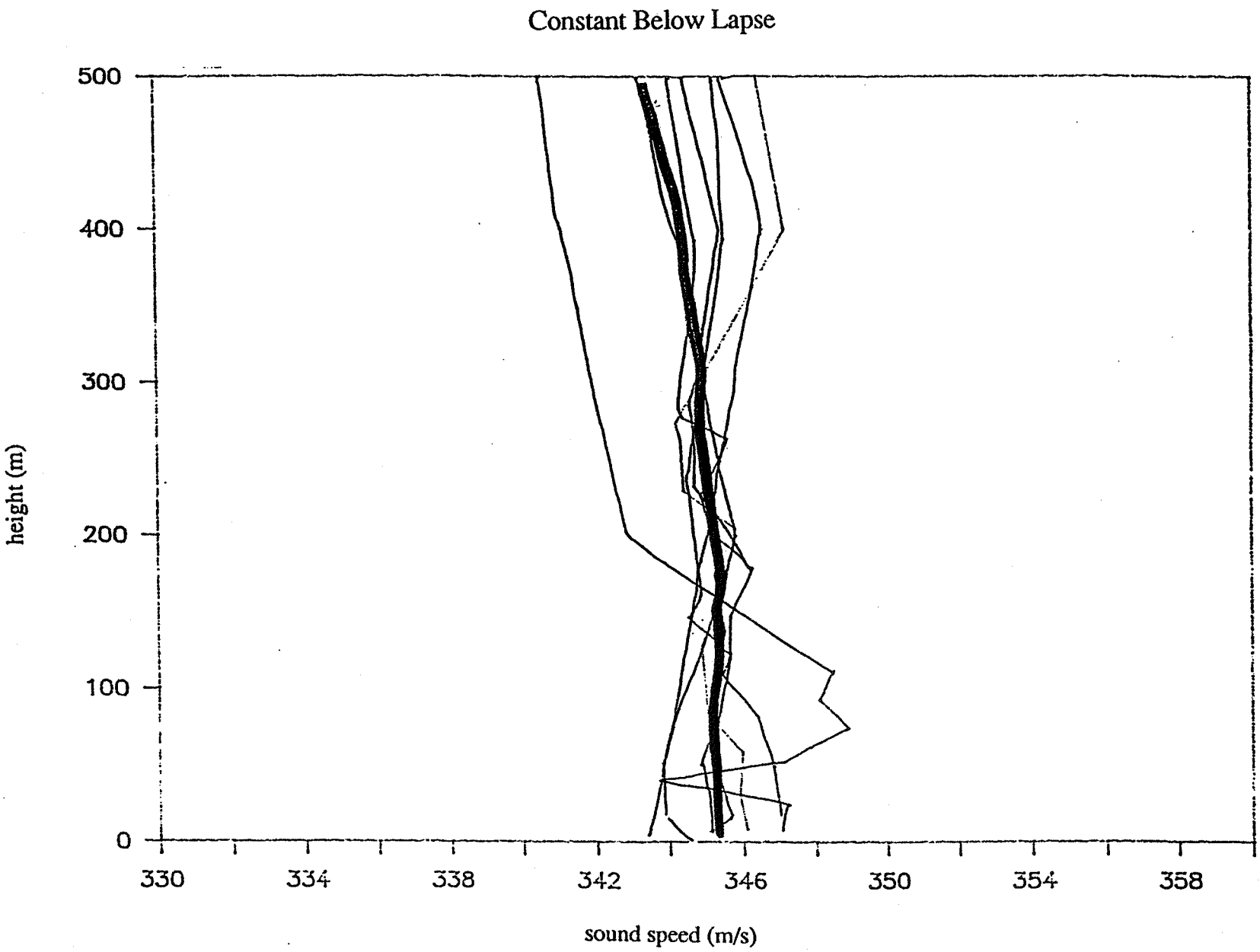

Figure 9. Sound velocity profiles for data from Ft. Bliss in the constant below lapse category. The heavy line indicates the average curve used in the FFP.

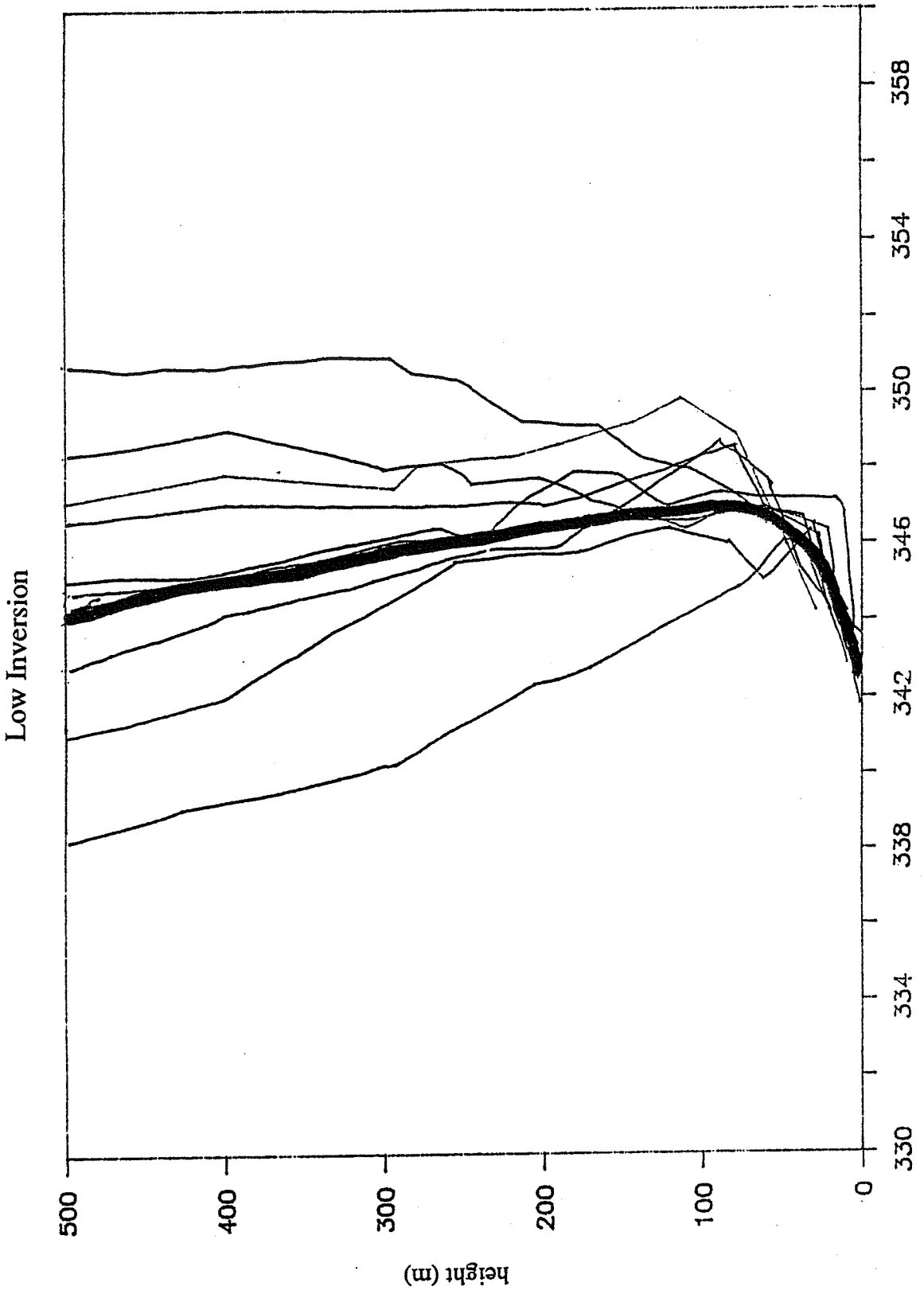

Figure 10. Sound velocity profiles for data from Ft. Bliss in the low inversion category. The heavy line indicates the average curve used in the FFP.

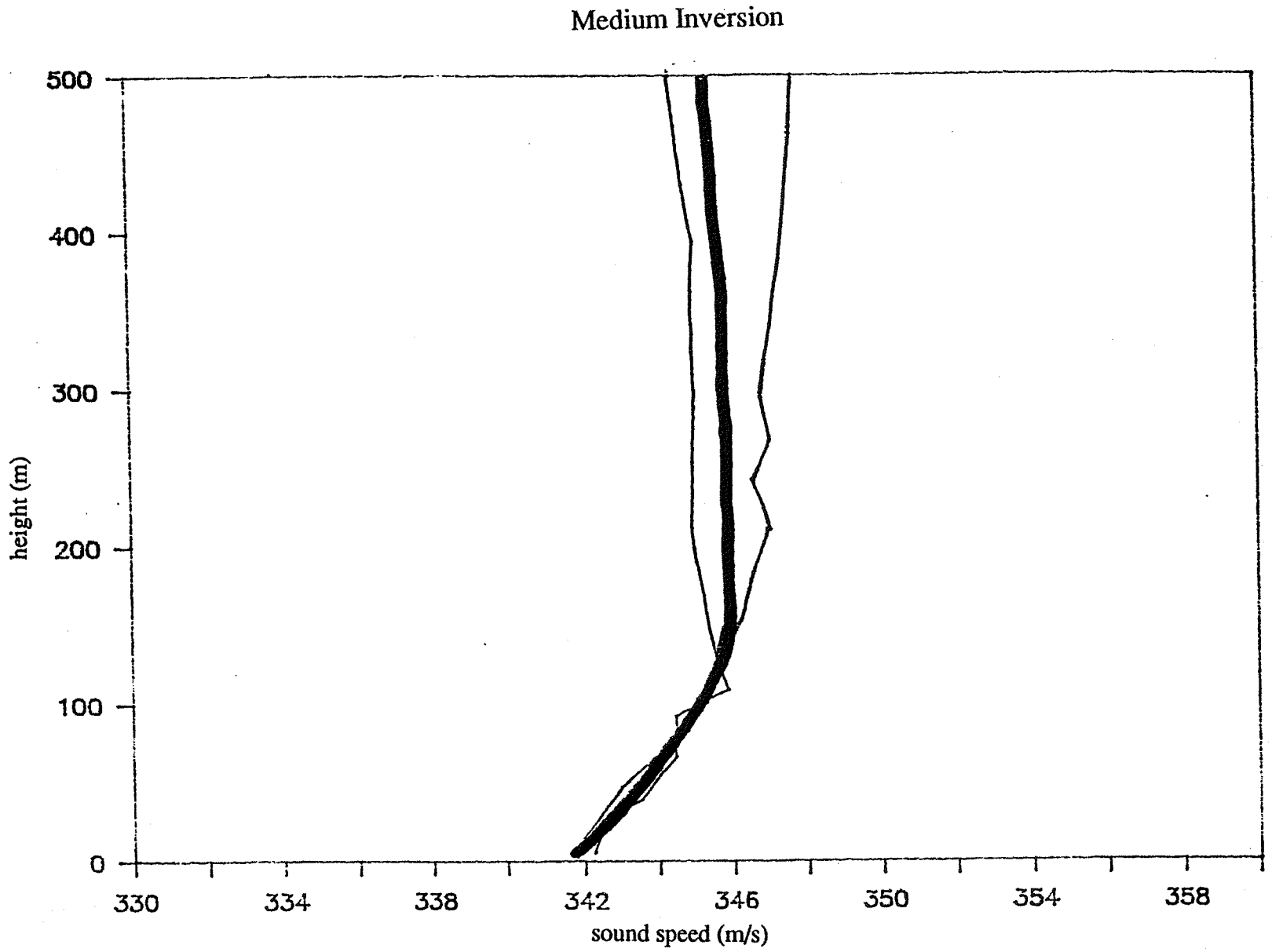

Figure 11. Sound velocity profiles for data from Ft. Bliss in the medium inversion category. The heavy line indicates the average curve used in the FFP.

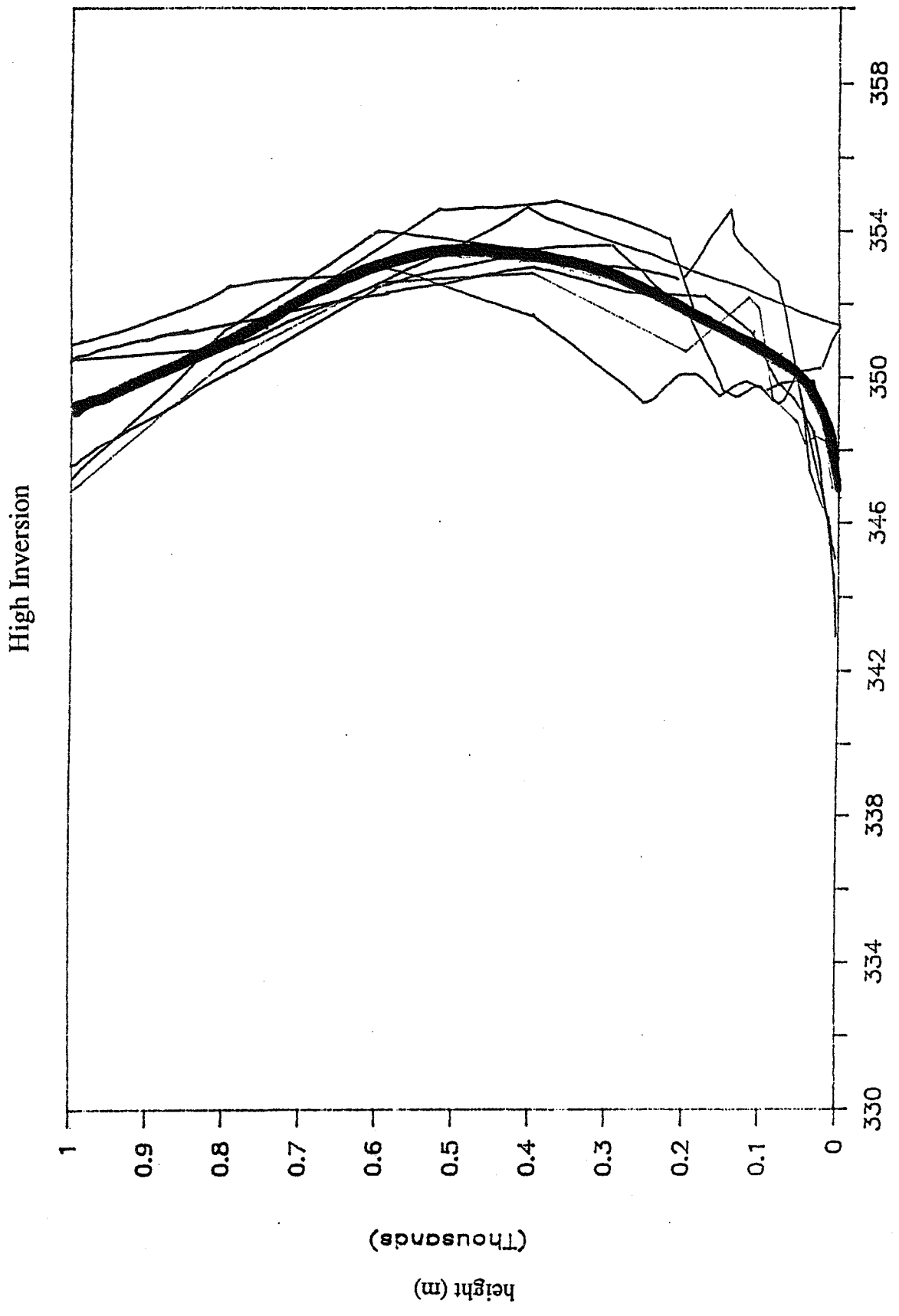

Figure 12. Sound velocity profiles for data from Ft. Bliss in the high inversion category. The heavy line indicates the average curve used in the FFP.

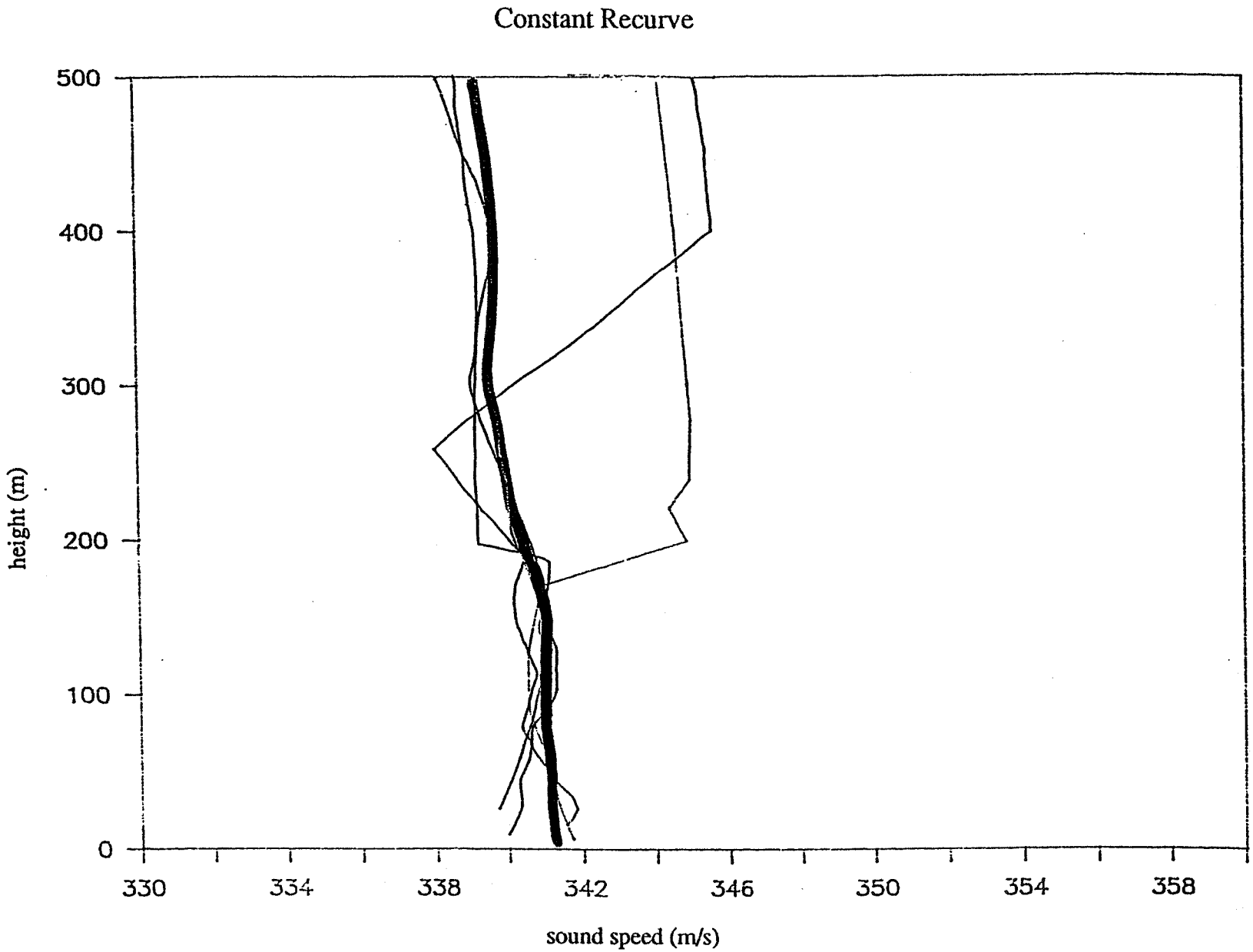

Figure 13. Sound velocity profiles for data from Ft. Bliss in the constant recurve category. The heavy line indicates the average curve used in the FFP.

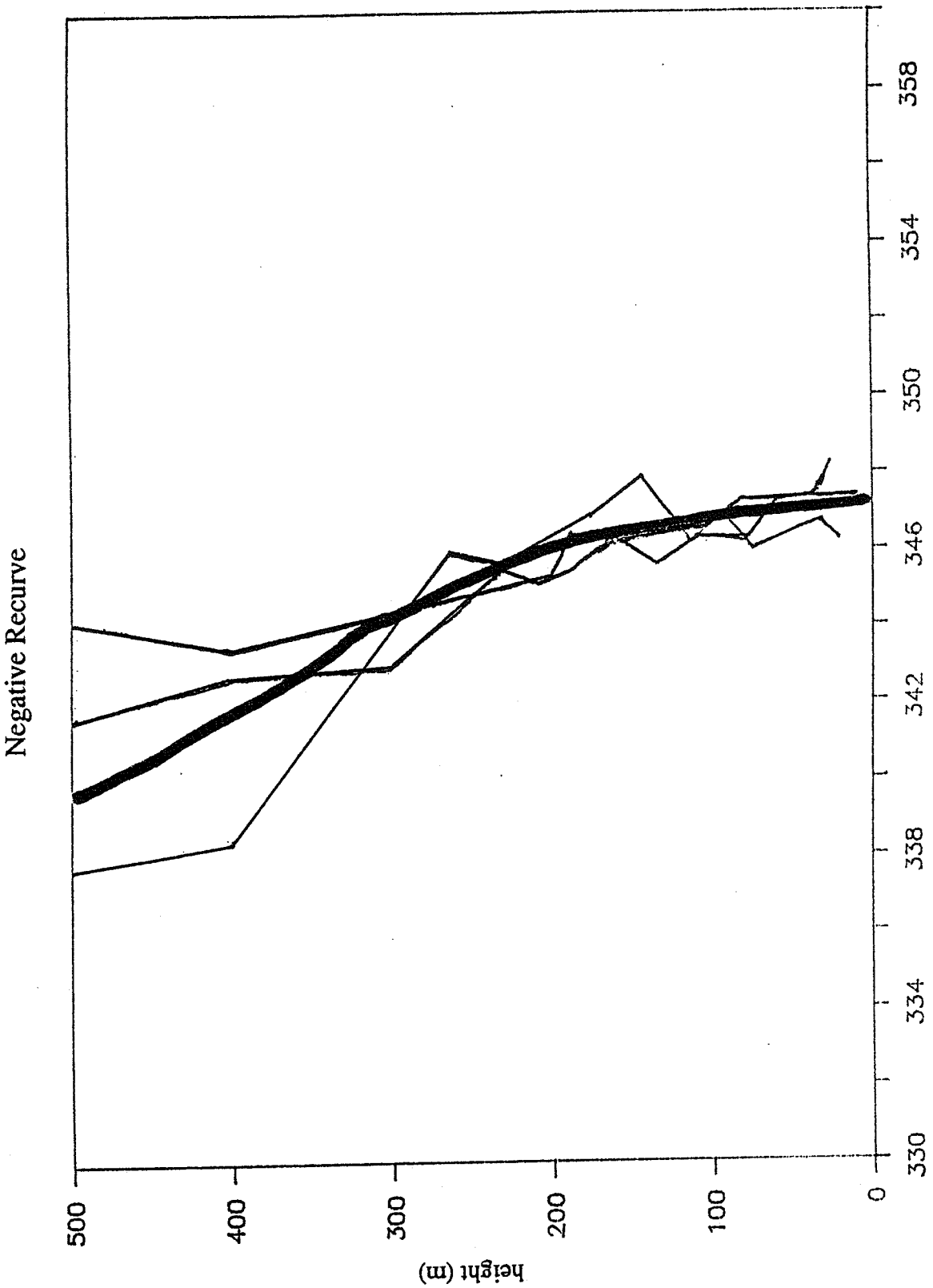

Figure 14. Sound velocity profiles for data from Ft. Bliss in the negative recurve category. The heavy line indicates the average curve used in the FFP.

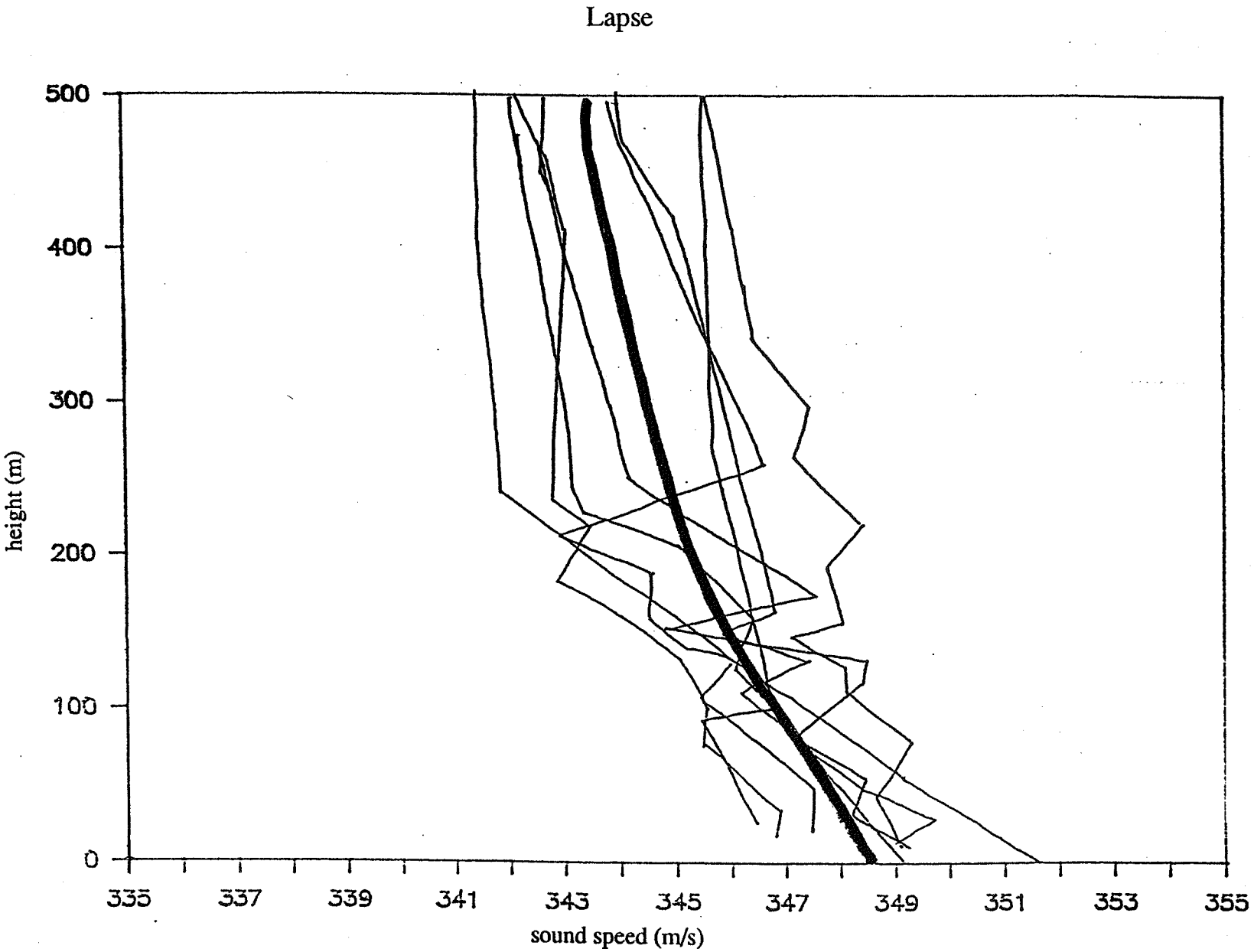

Figure 15. Sound velocity profiles for data from Aberdeen Proving Ground in the lapse category. The heavy line indicates the average curve used in the FFP.

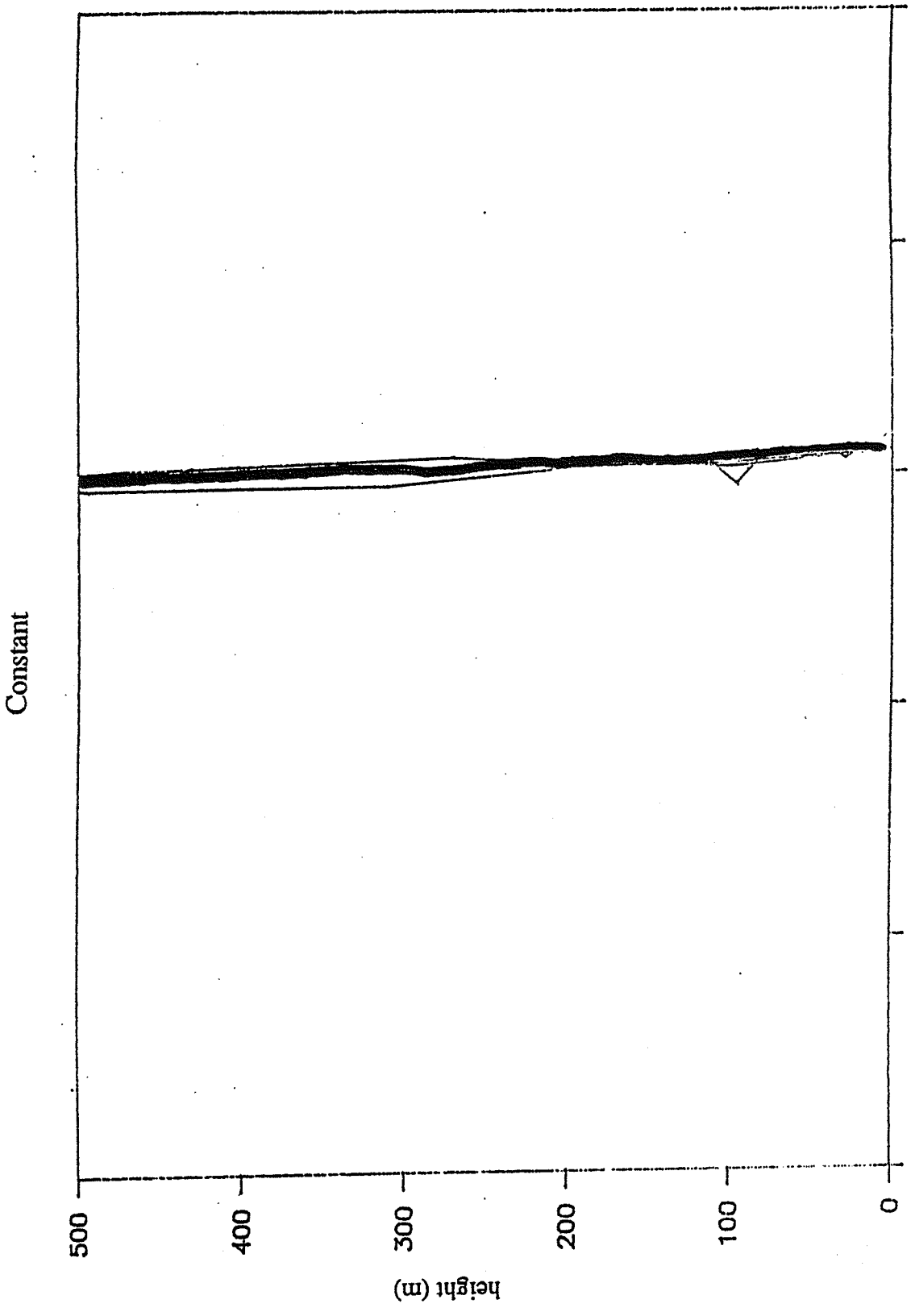

Figure 16. Sound velocity profiles for data from Aberdeen Proving Ground in the constant category. The heavy line indicates the average curve used in the FFP.

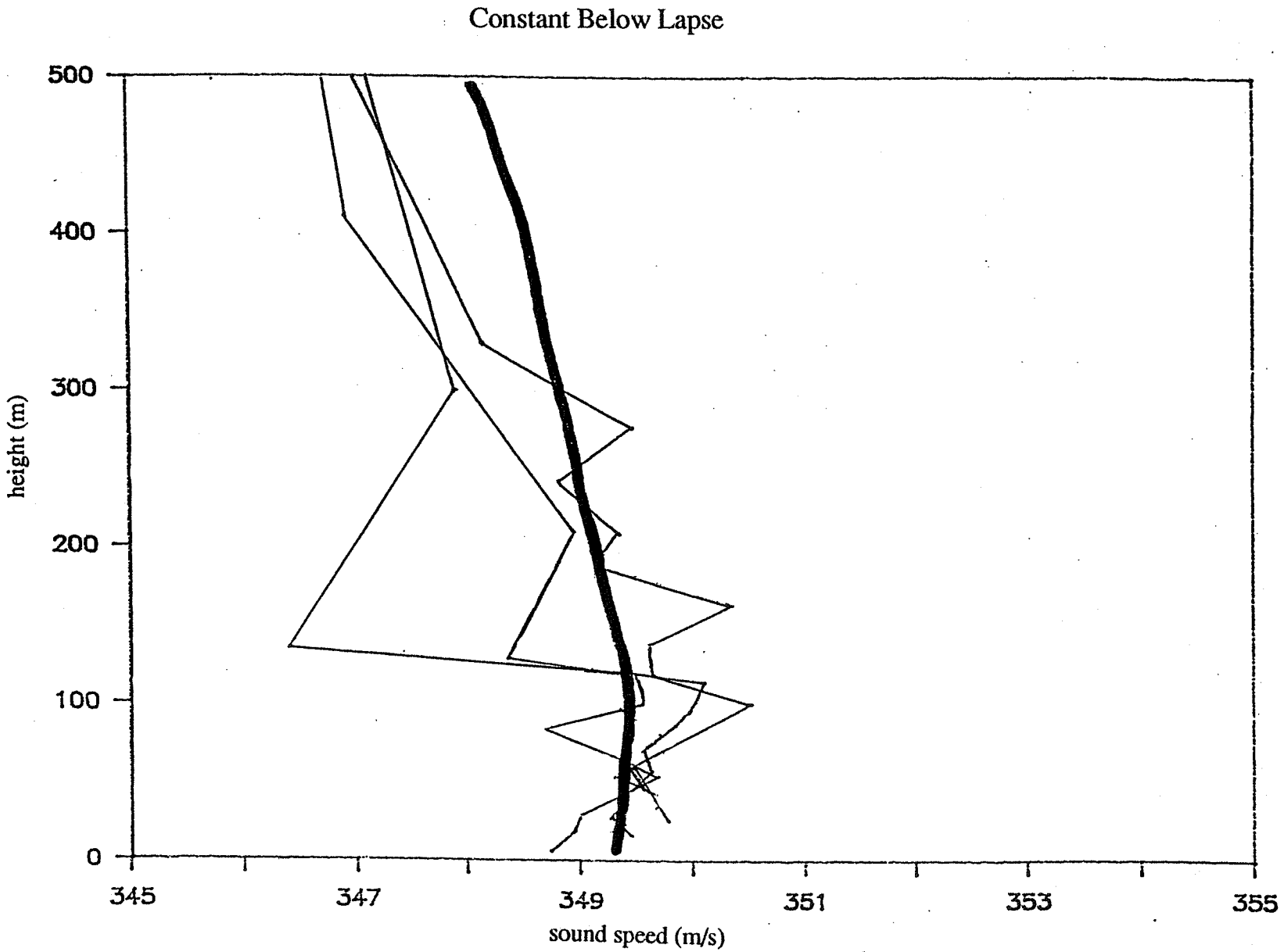

Figure 17. Sound velocity profiles for data from Aberdeen Proving Ground in the constant below lapse category. The heavy line indicates the average curve used in the FFP.

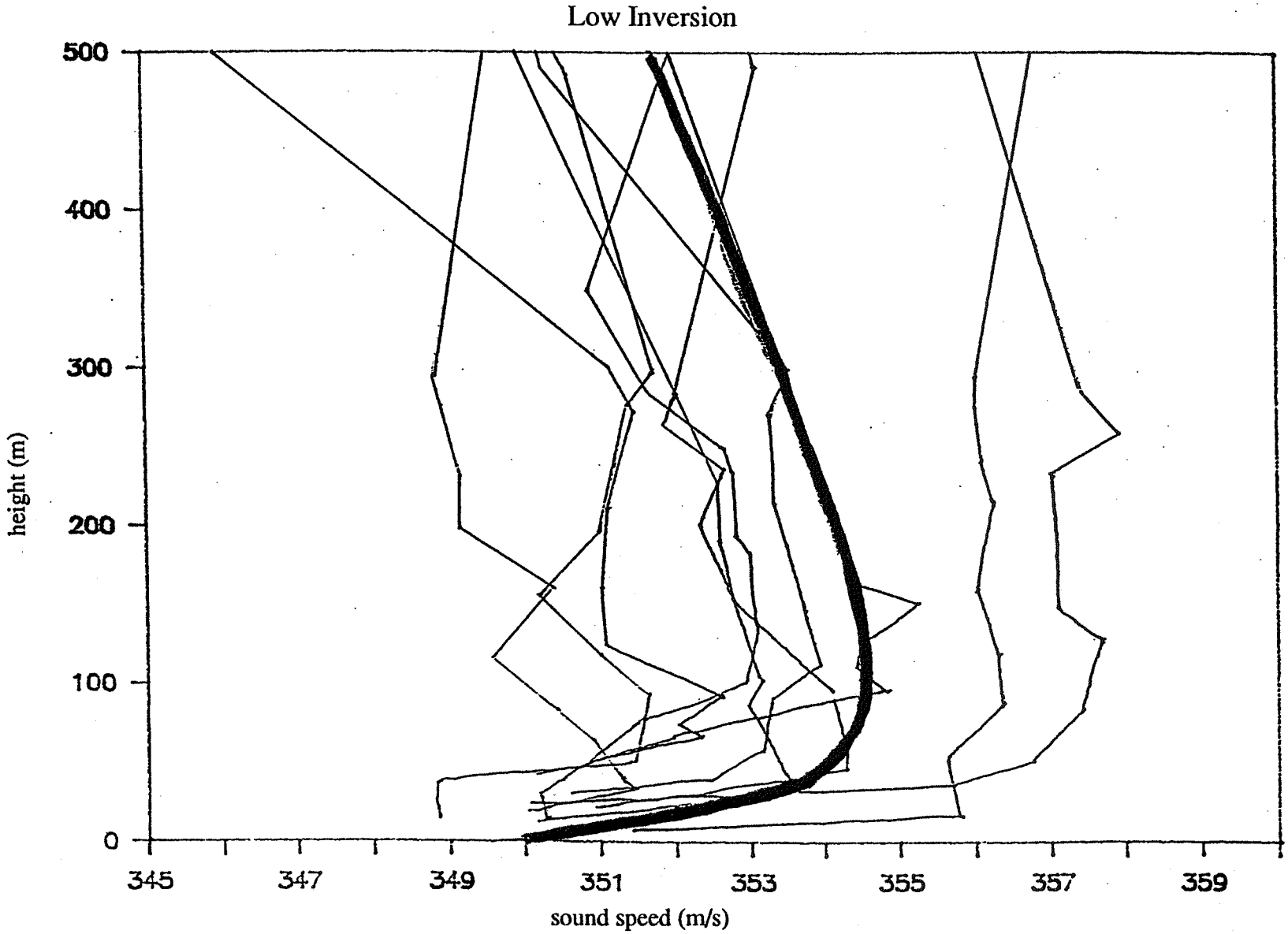

Figure 18. Sound velocity profiles for data from Aberdeen Proving Ground in the low inversion category. The heavy line indicates the average curve used in the FFP.

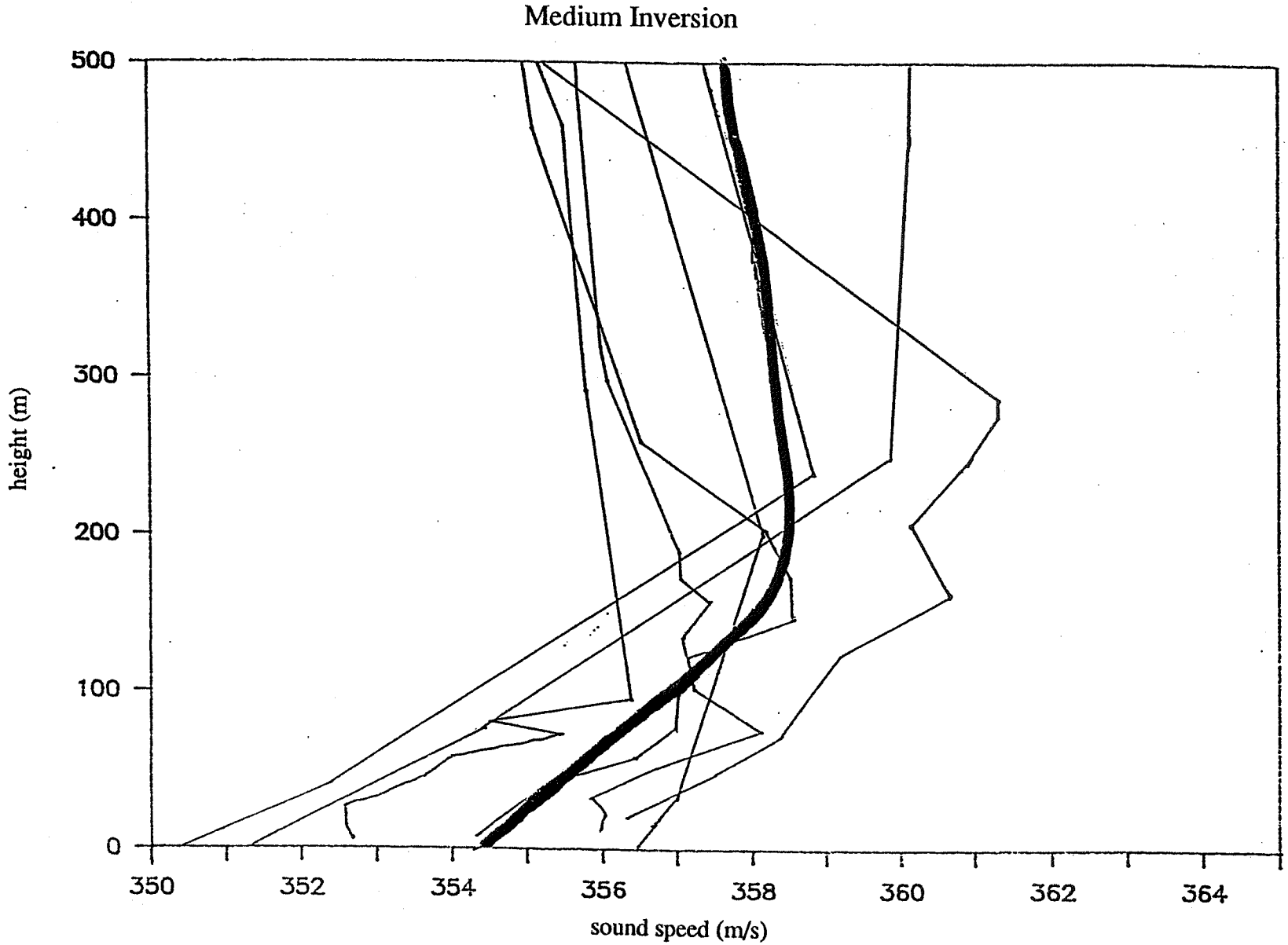

Figure 19. Sound velocity profiles for data from Aberdeen Proving Ground in the medium inversion category. The heavy line indicates the average curve used in the FFP.

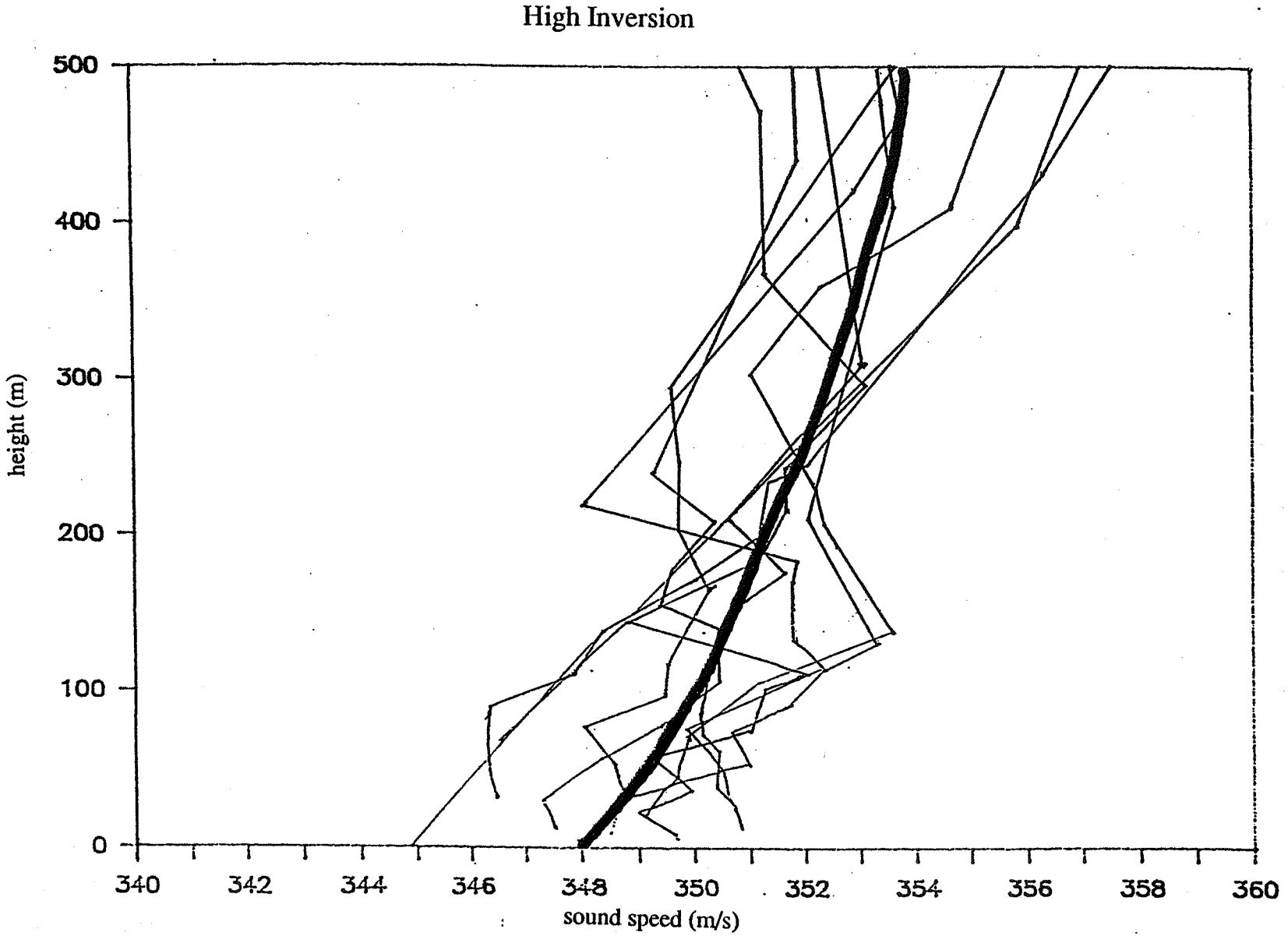

Figure 20. Sound velocity profiles for data from Aberdeen Proving Ground in the high inversion category. The heavy line indicates the average curve used in the FFP.

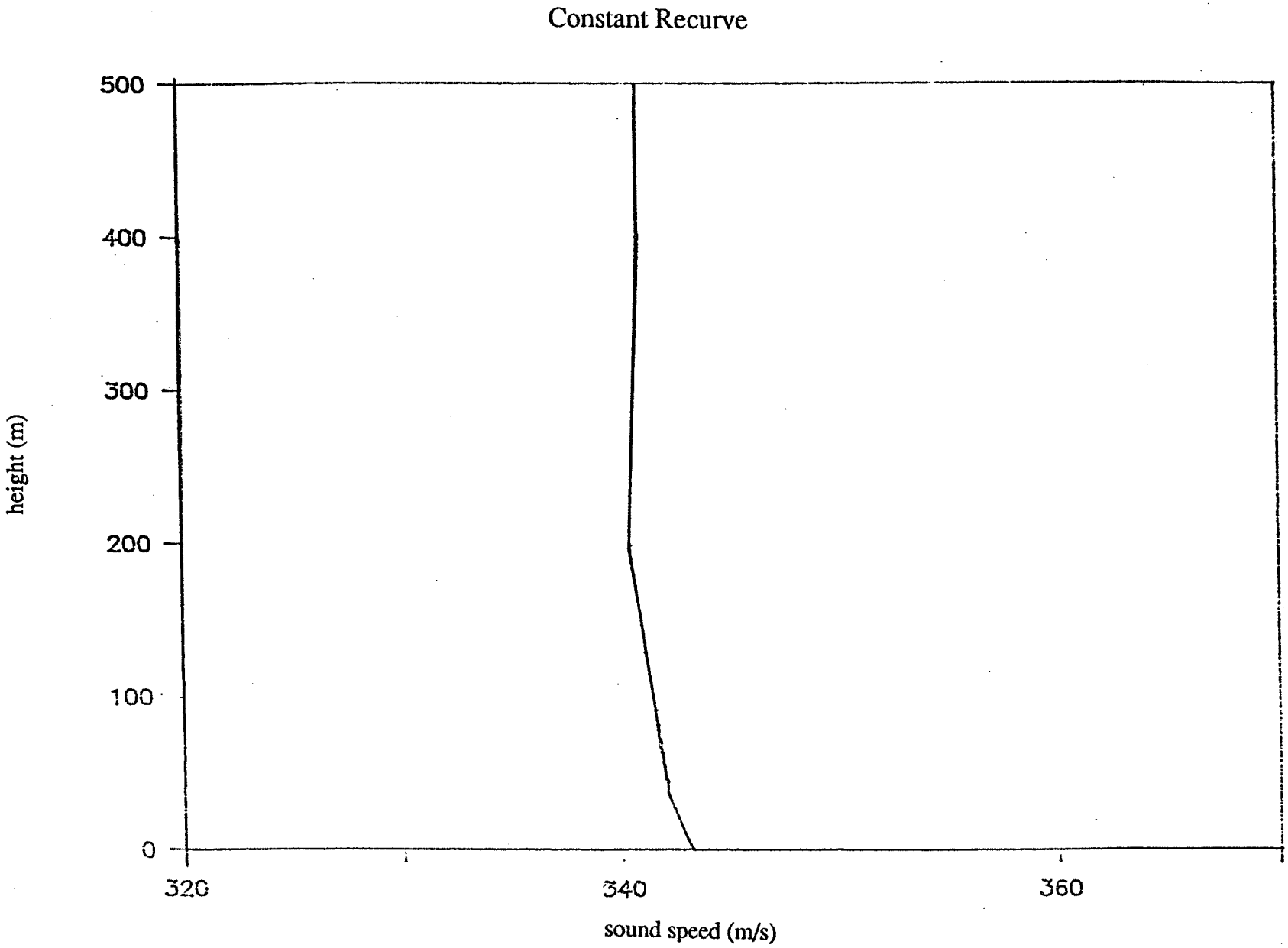

Figure 21. Sound velocity profiles for data from Aberdeen Proving Ground in the constant recurve category. The heavy line indicates the average curve used in the FFP.

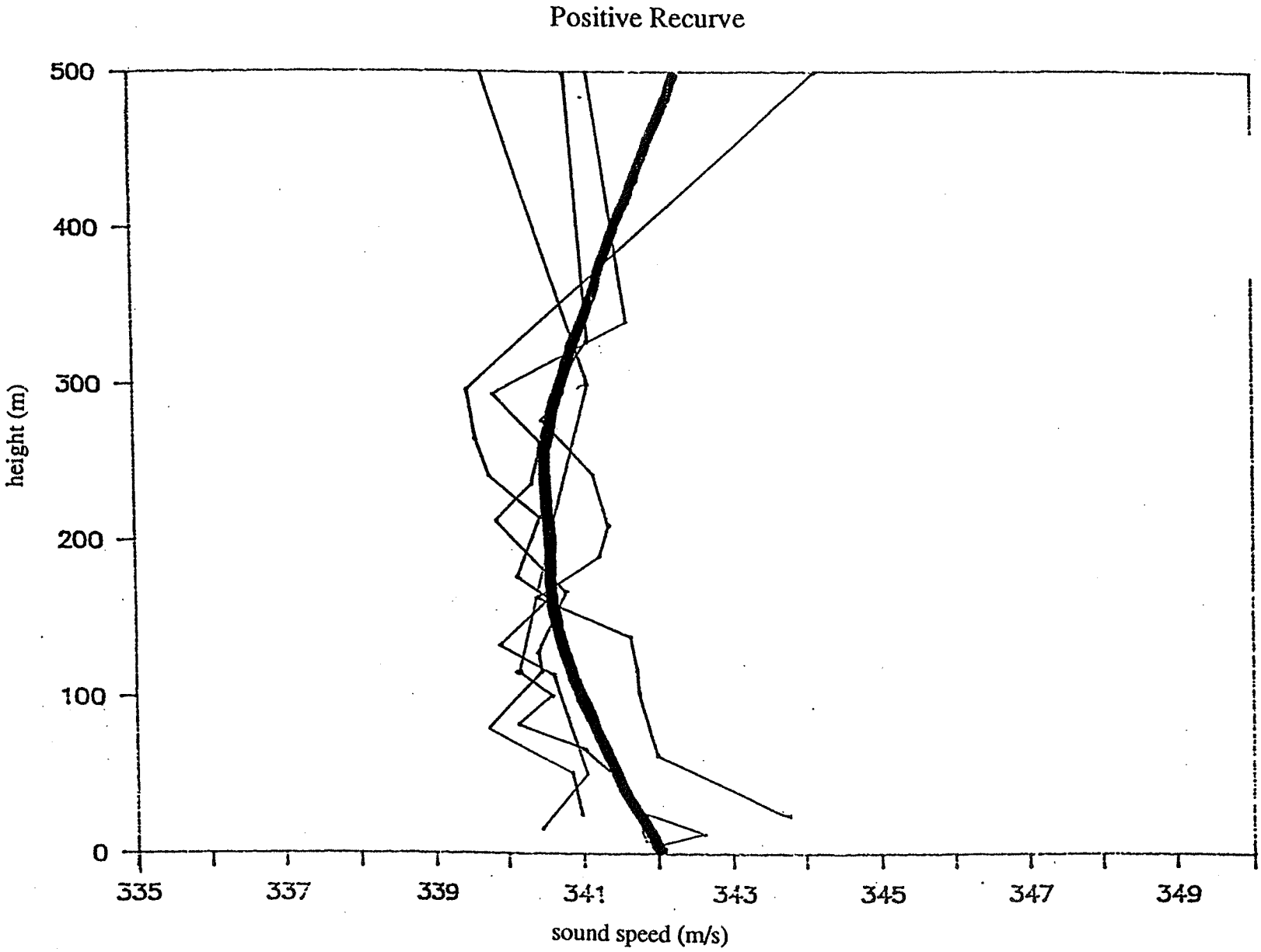

Figure 22. Sound velocity profiles for data from Aberdeen Proving Ground in the positive recurve category. The heavy line indicates the average curve used in the FFP.

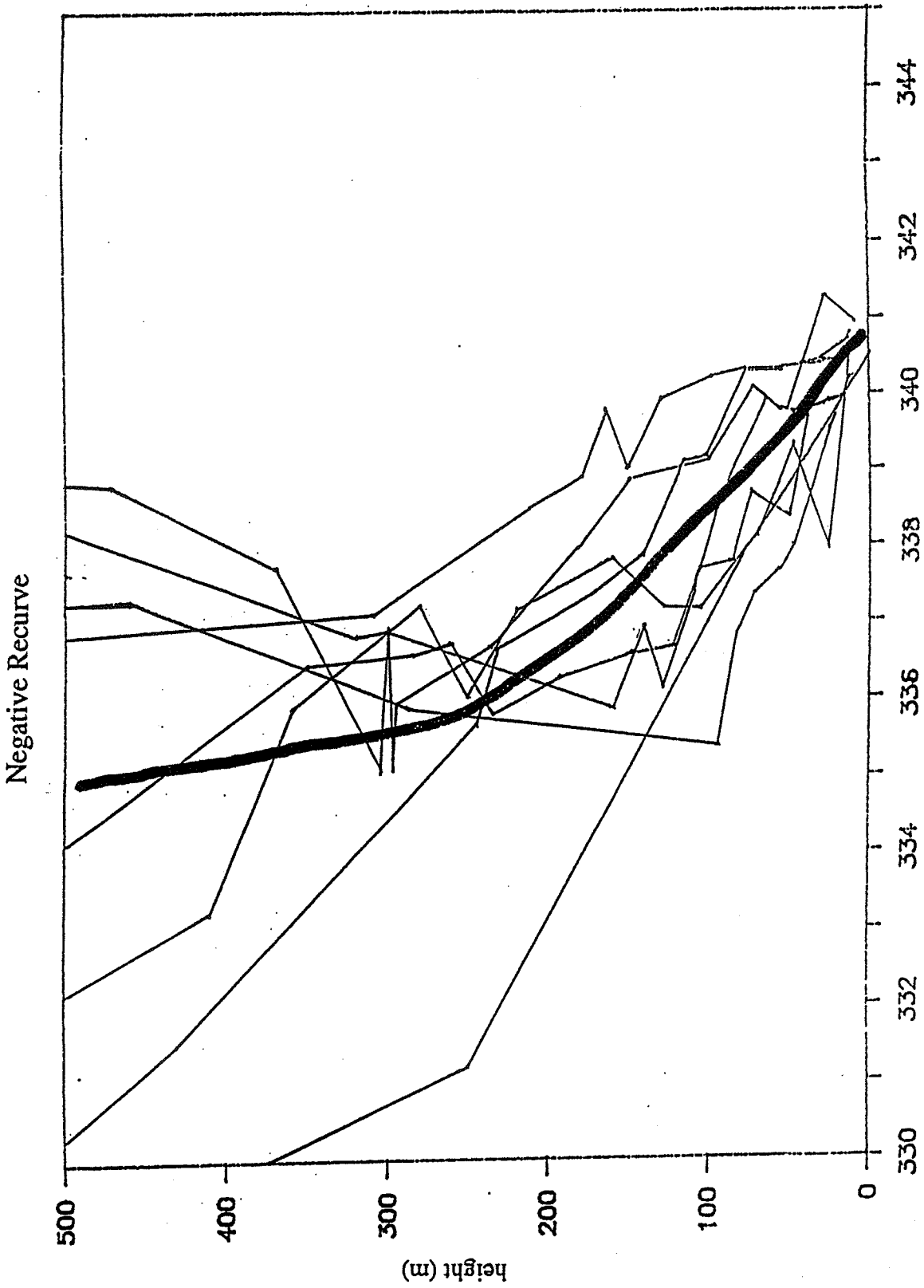

Figure 23. Sound velocity profiles for data from Aberdeen Proving Ground in the negative recurve catagory. The heavy line indicates the average curve used in the FFP.

VII. RESULTS

The results of running the average curve in a 12-layer FFP run for each category are shown with the actual sound exposure levels recorded at each measurement site in Figures 24-31 for Ft. Bliss and Figures 32-40 for Aberdeen Proving Ground. Figures appear at end of Chapter VII. Over soil (Ft. Bliss), the flow resistance was taken to be 100 cgs Rayls. Over water (Aberdeen), the impedance was taken as real with $Z = \rho c$, where the sound speed in water was 1500 m/s and had a density of 998 kg/m^3. The flow resistance was assumed to be zero.

Each circle represents one reading of CSEL taken at the corresponding distance. The solid line represents the CSEL predicted by the FFP. All graphs are for 1 1/4 pound charges.

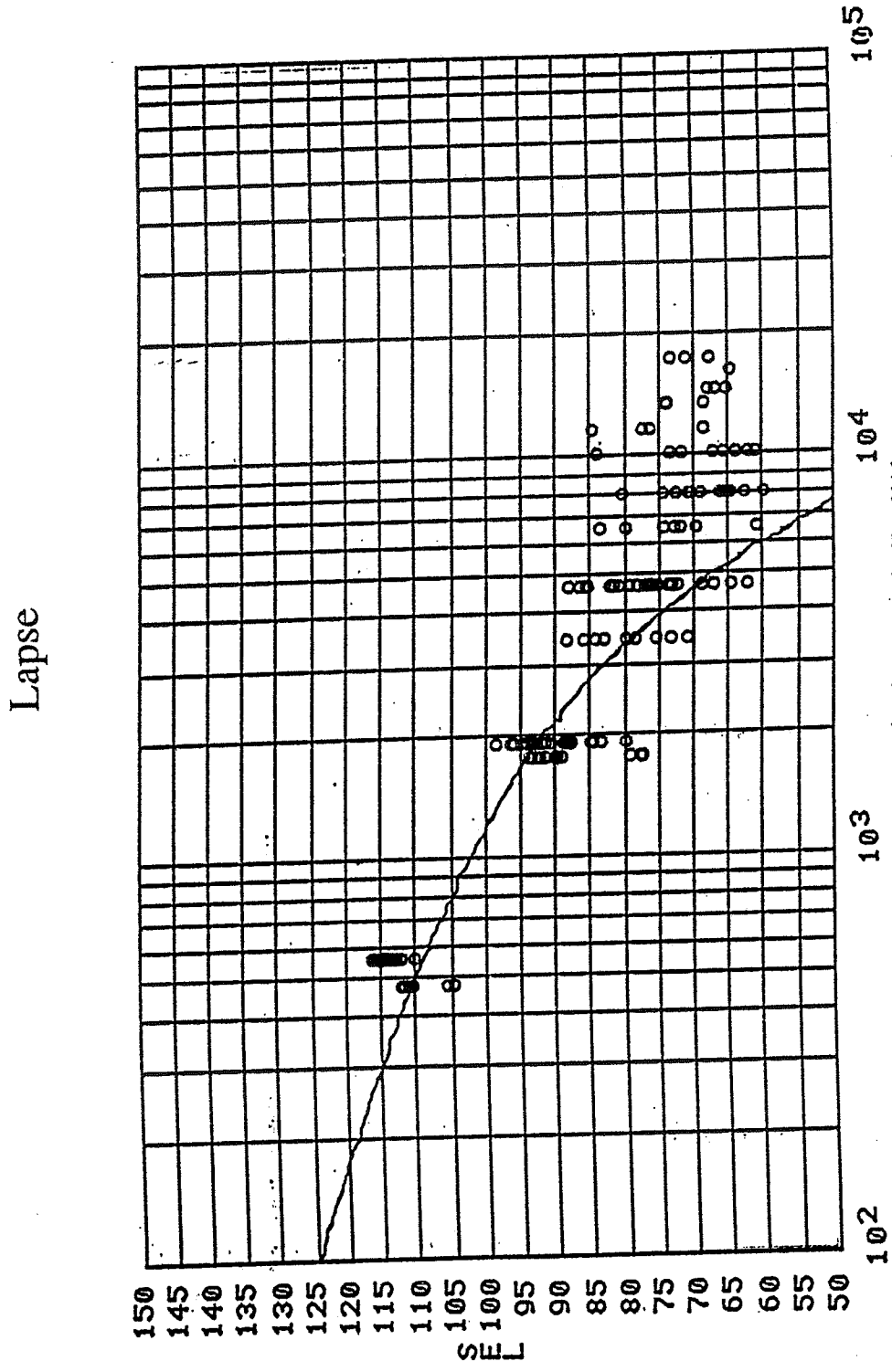

Figure 24. CSEL vs. distance for lapse category data from Ft. Bliss and FFP output.

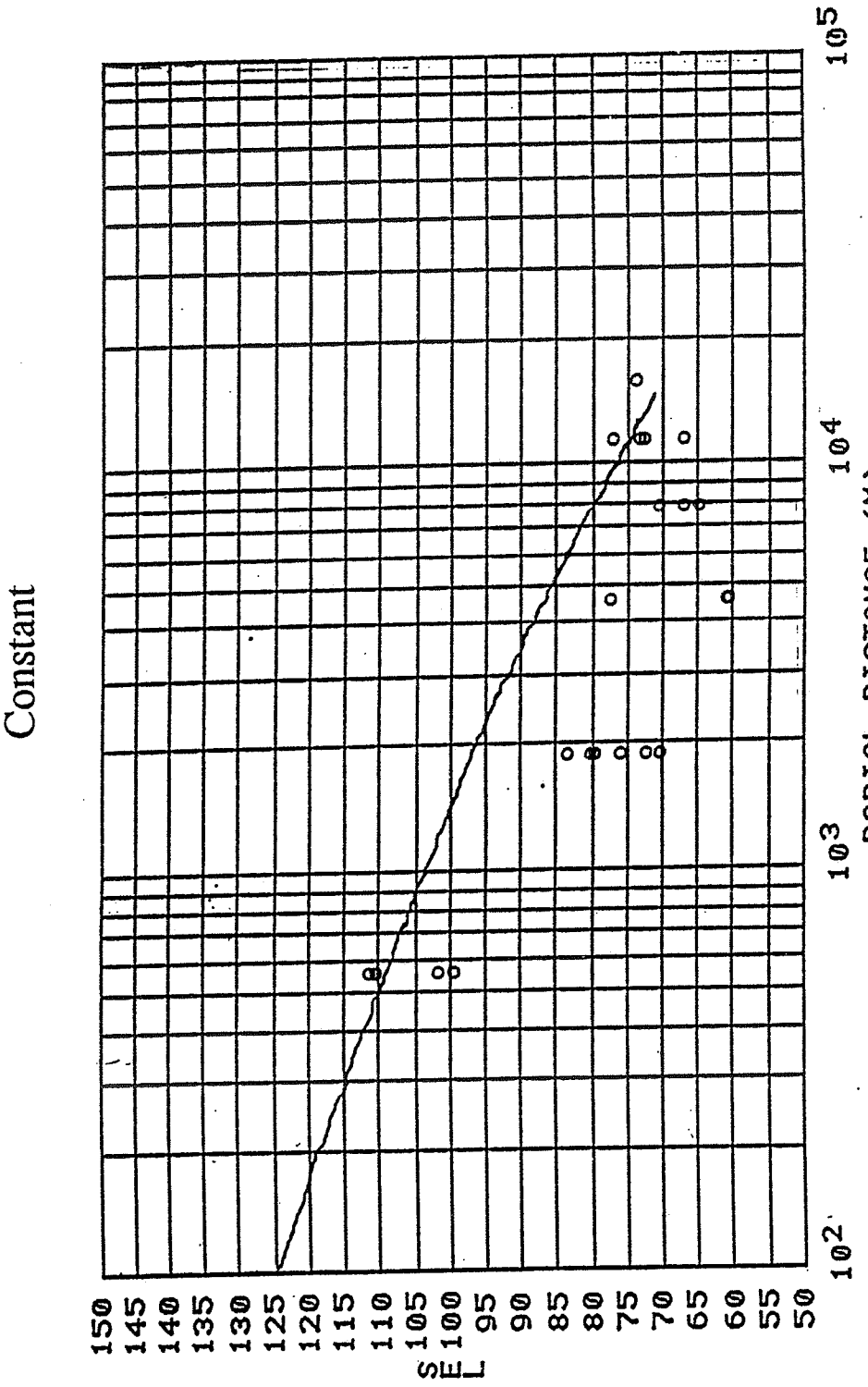

Figure 25. CSEL vs. distance for constant category data from Ft. Bliss and FFP output.

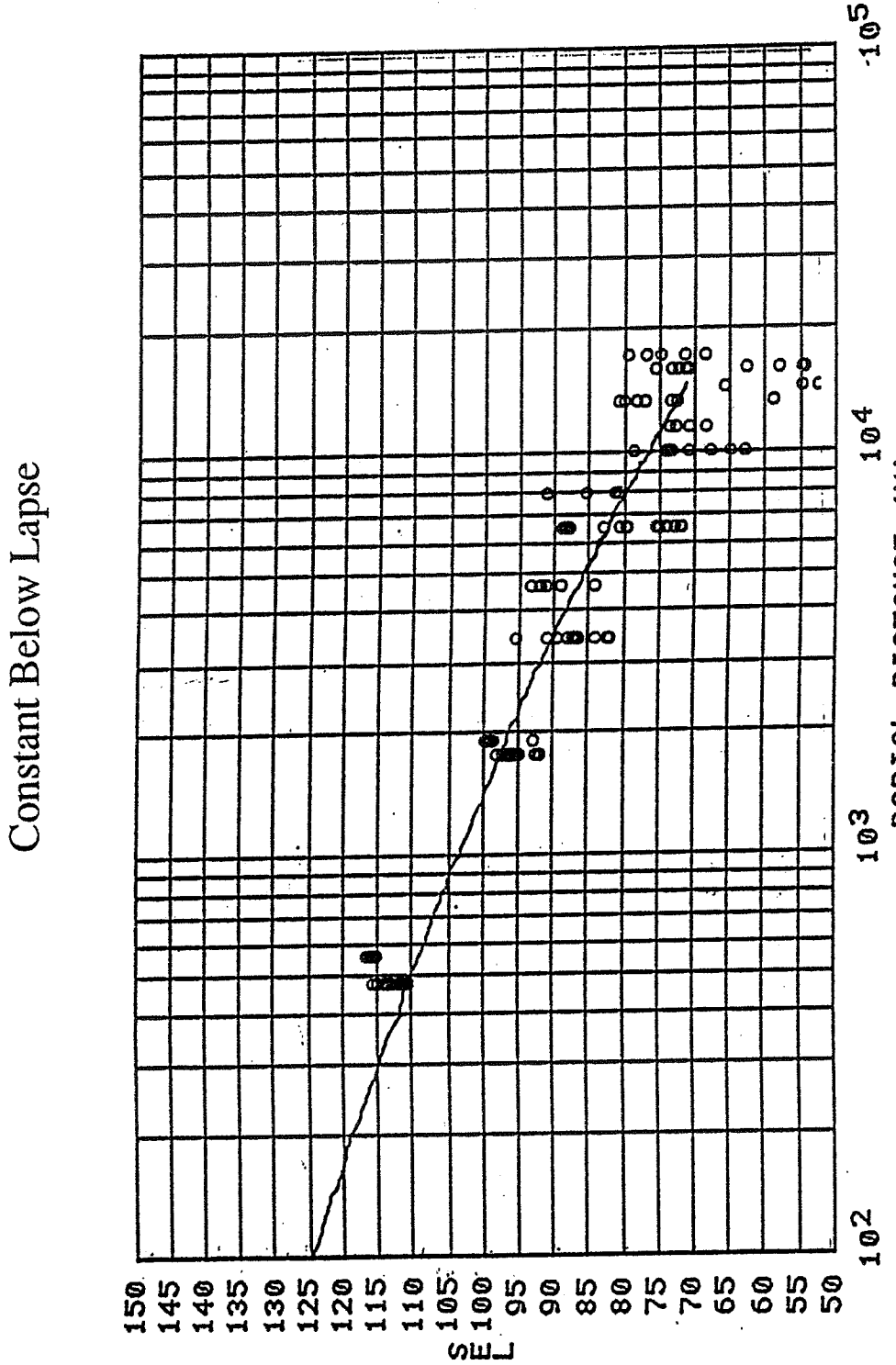

Figure 26. CSEL vs. distance for constant below lapse category data from Ft. Bliss and FFP output.

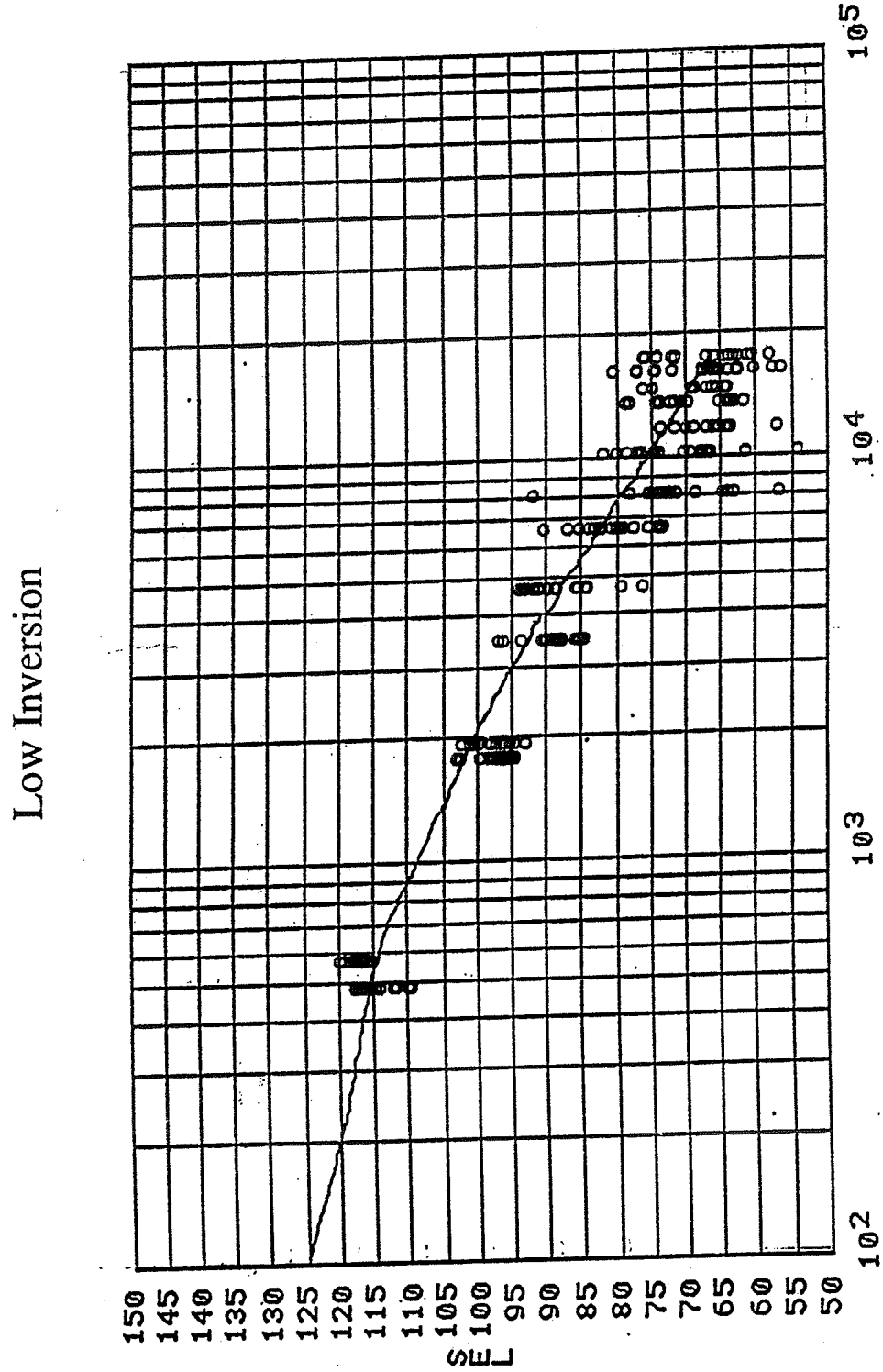

Figure 27. CSEL vs. distance for low inversion category data from Ft. Bliss and FFP output.

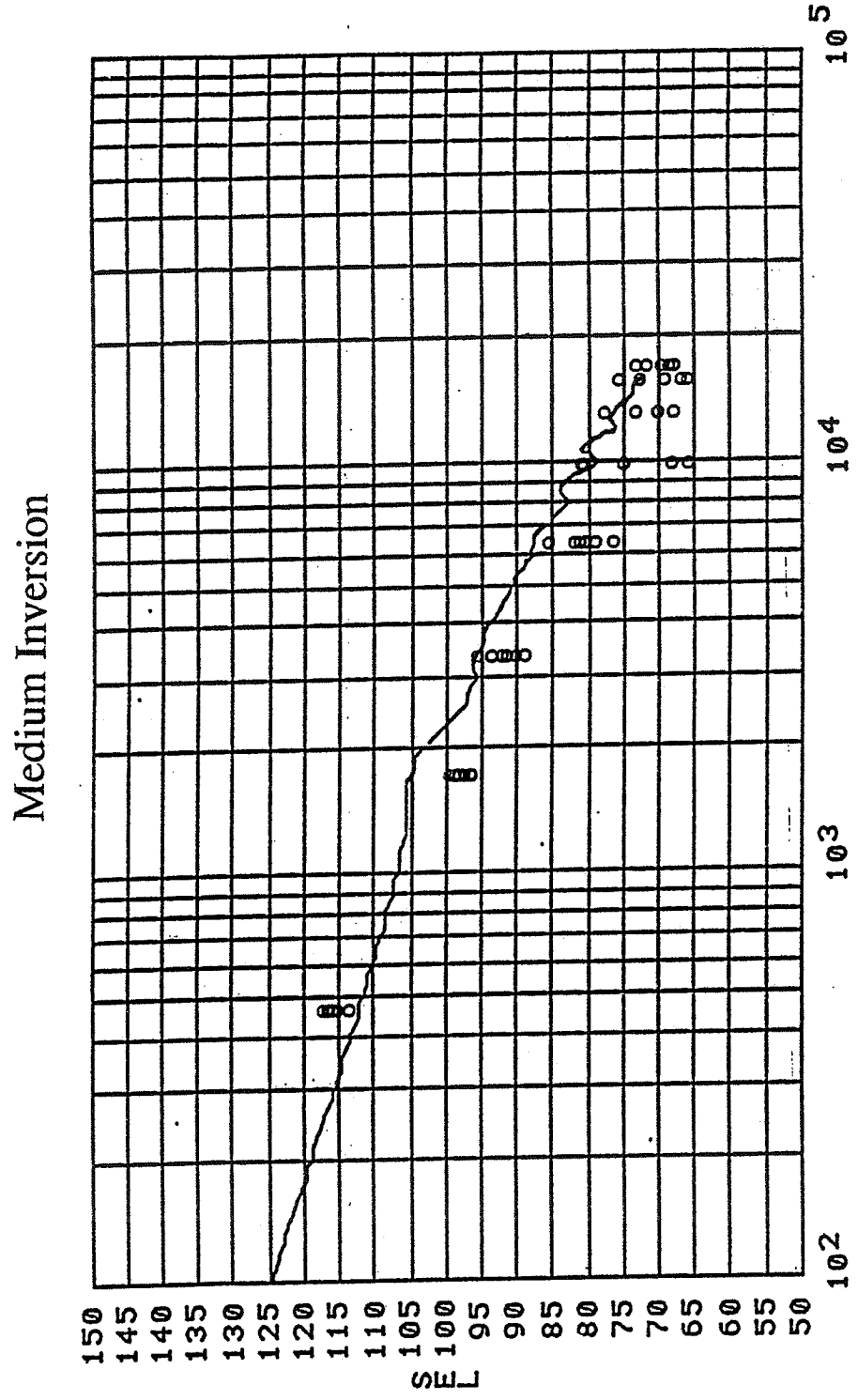

Figure 28. CSEL vs. distance for medium inversion category data from Ft. Bliss and FFP output.

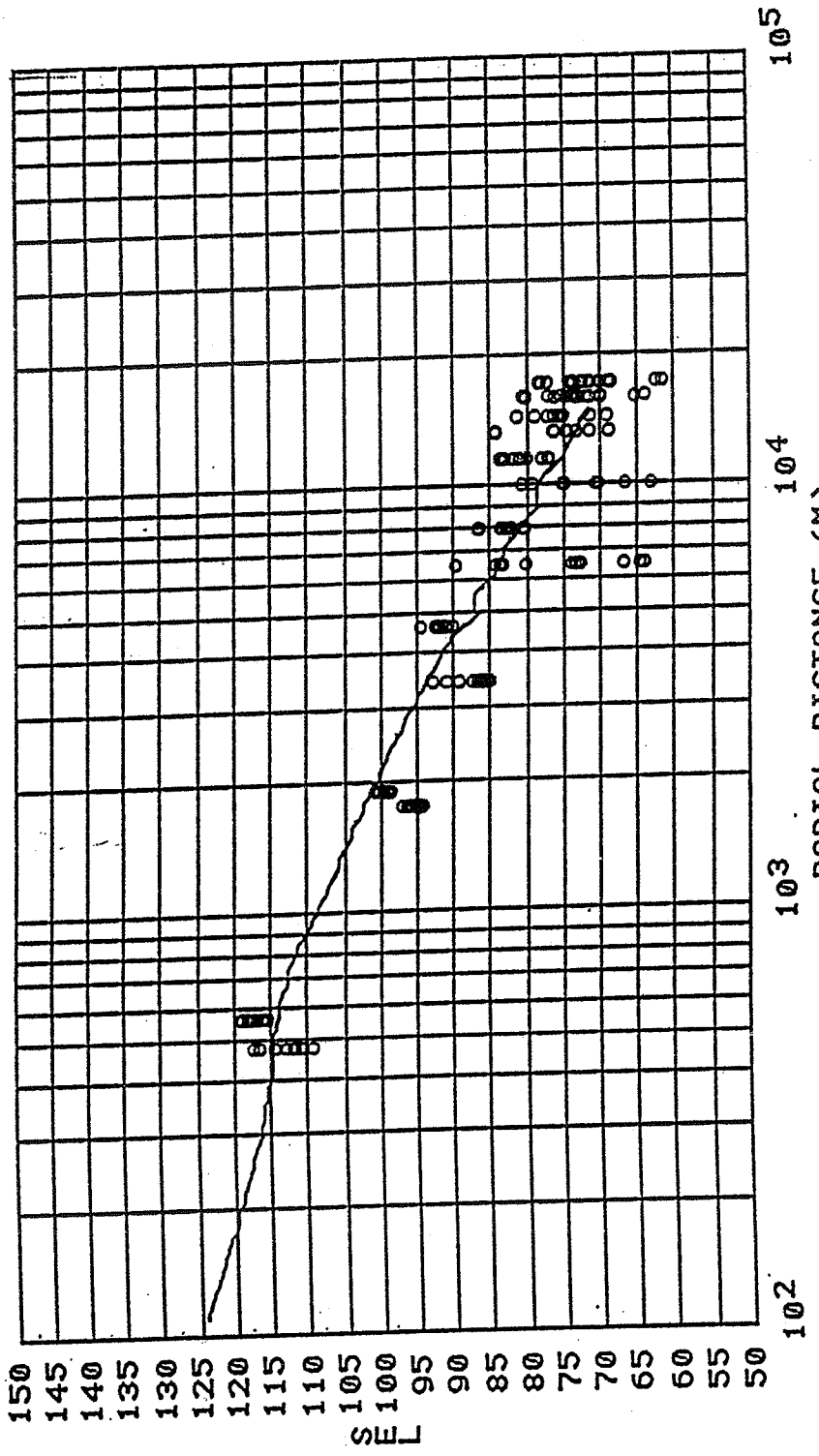

Figure 29. CSEL vs. distance for high inversion category data from Ft. Bliss and FFP output.

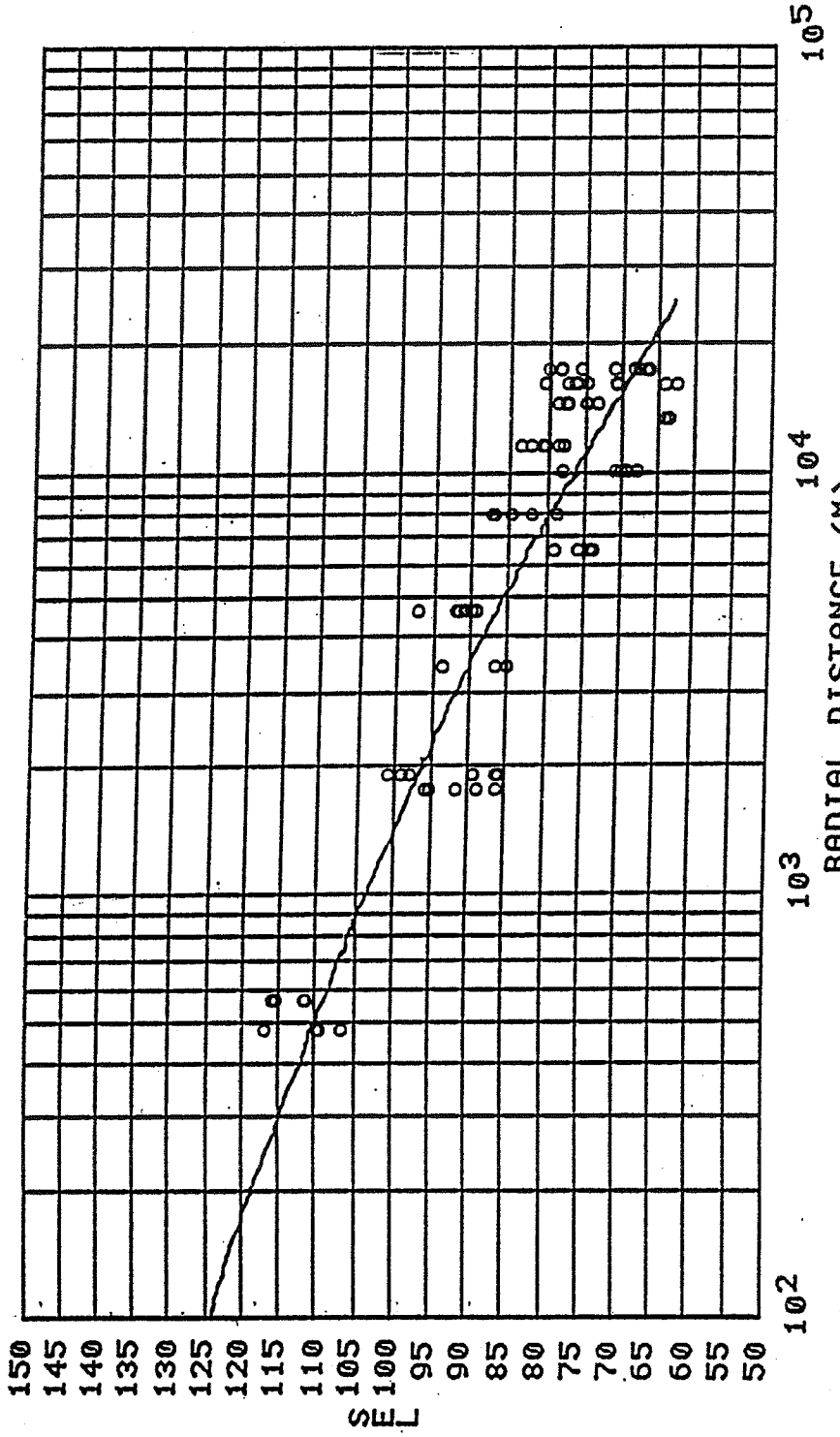

Figure 30. CSEL vs. distance for constant recurve category data from Ft. Bliss and FFP output.

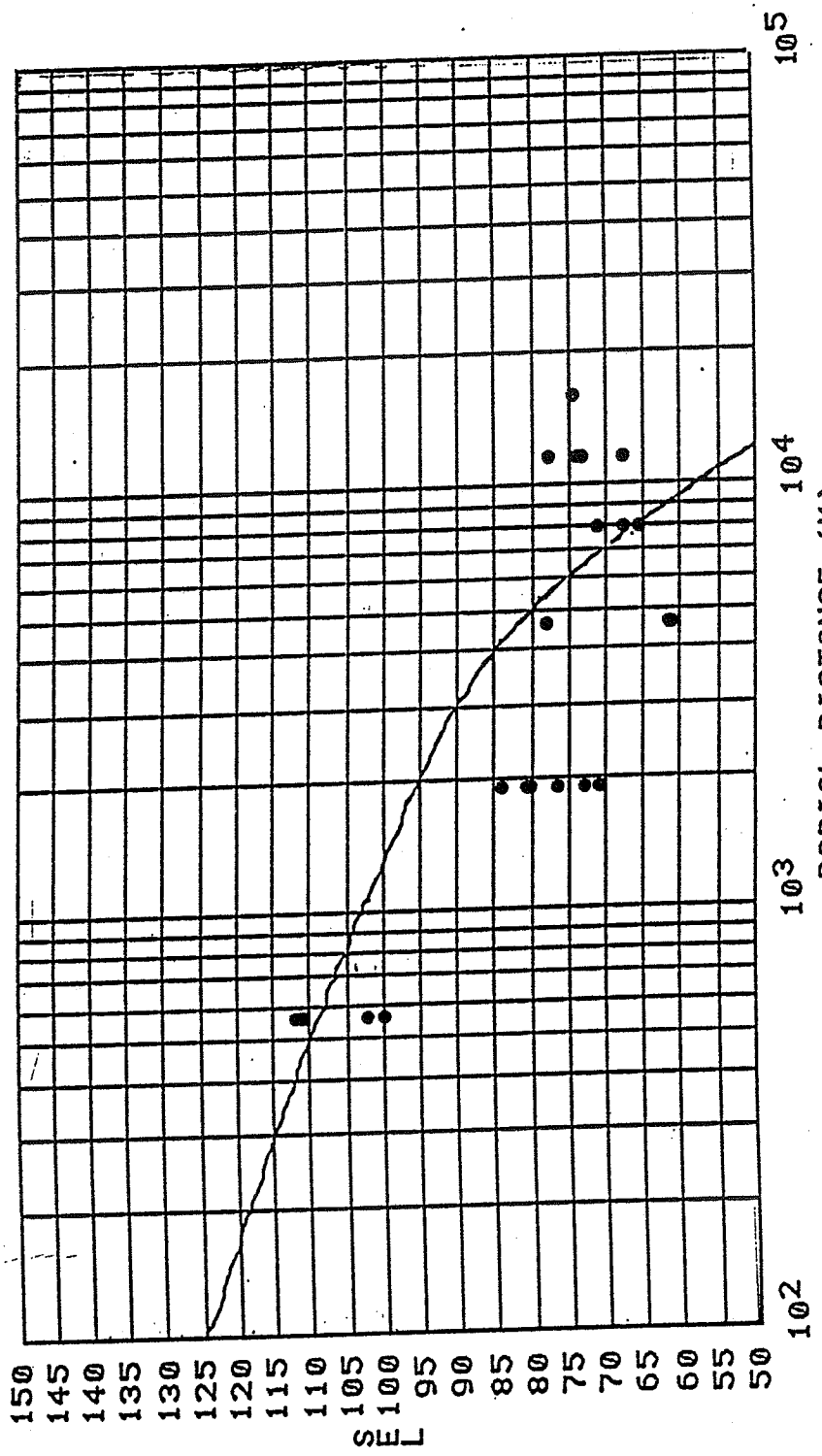

Figure 31. CSEL vs. distance for negative recurve category data from Ft. Bliss and FFP output.

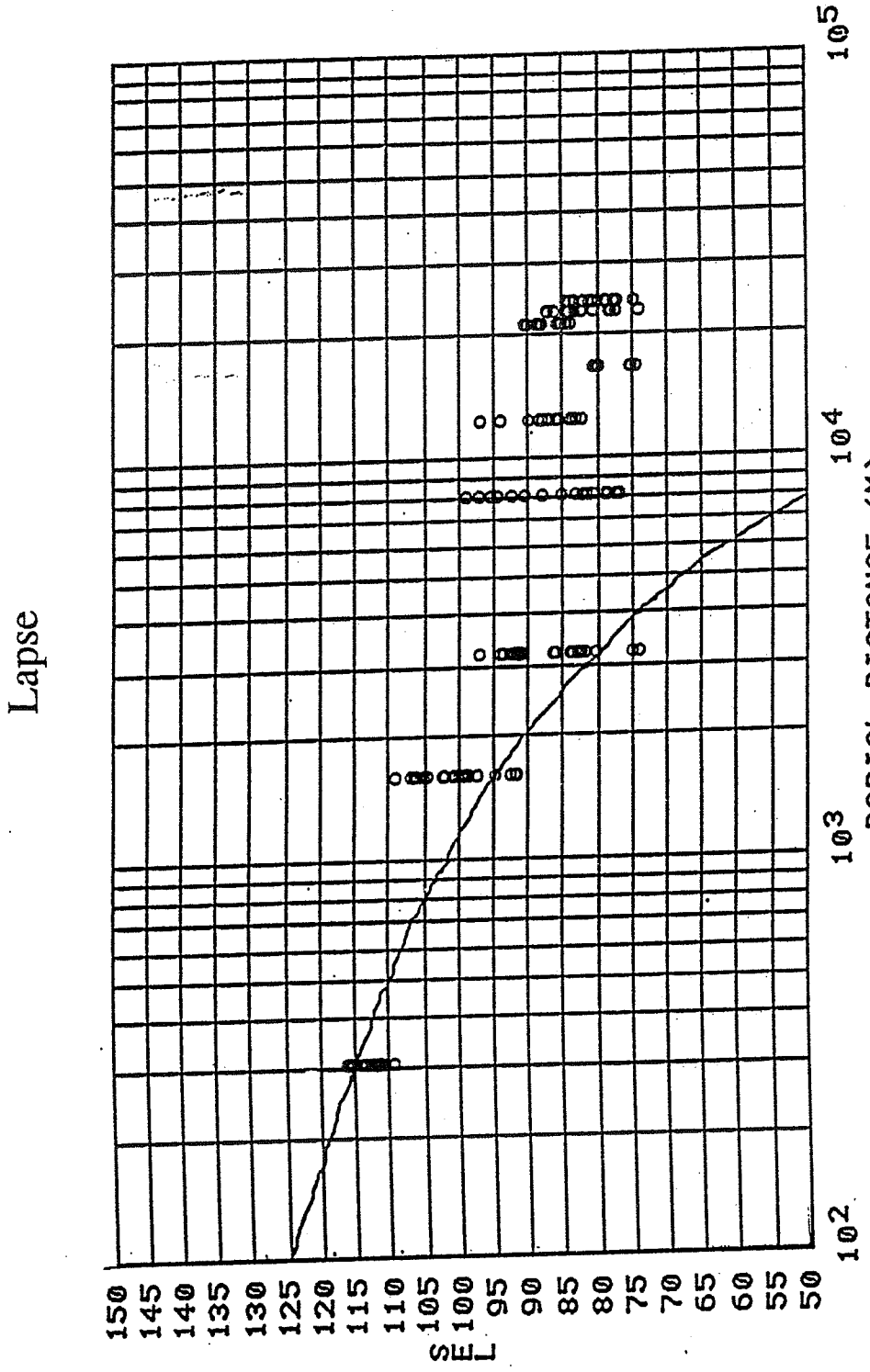

Figure 32. CSEL vs. distance for lapse category data from Aberdeen Proving Ground and FFP output.

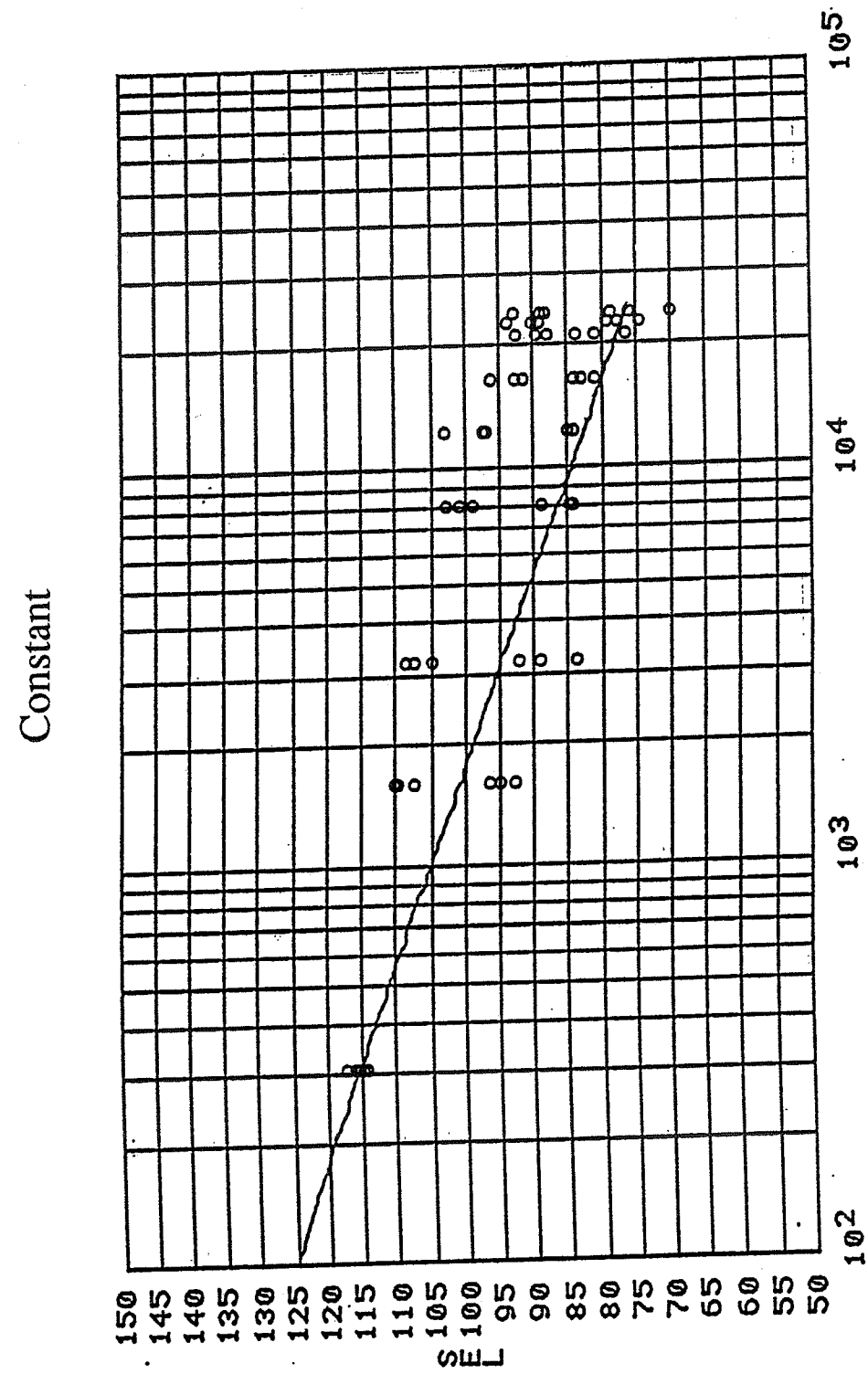

Figure 33. CSEL vs. distance for constant category data from Aberdeen Proving Ground and FFP output.

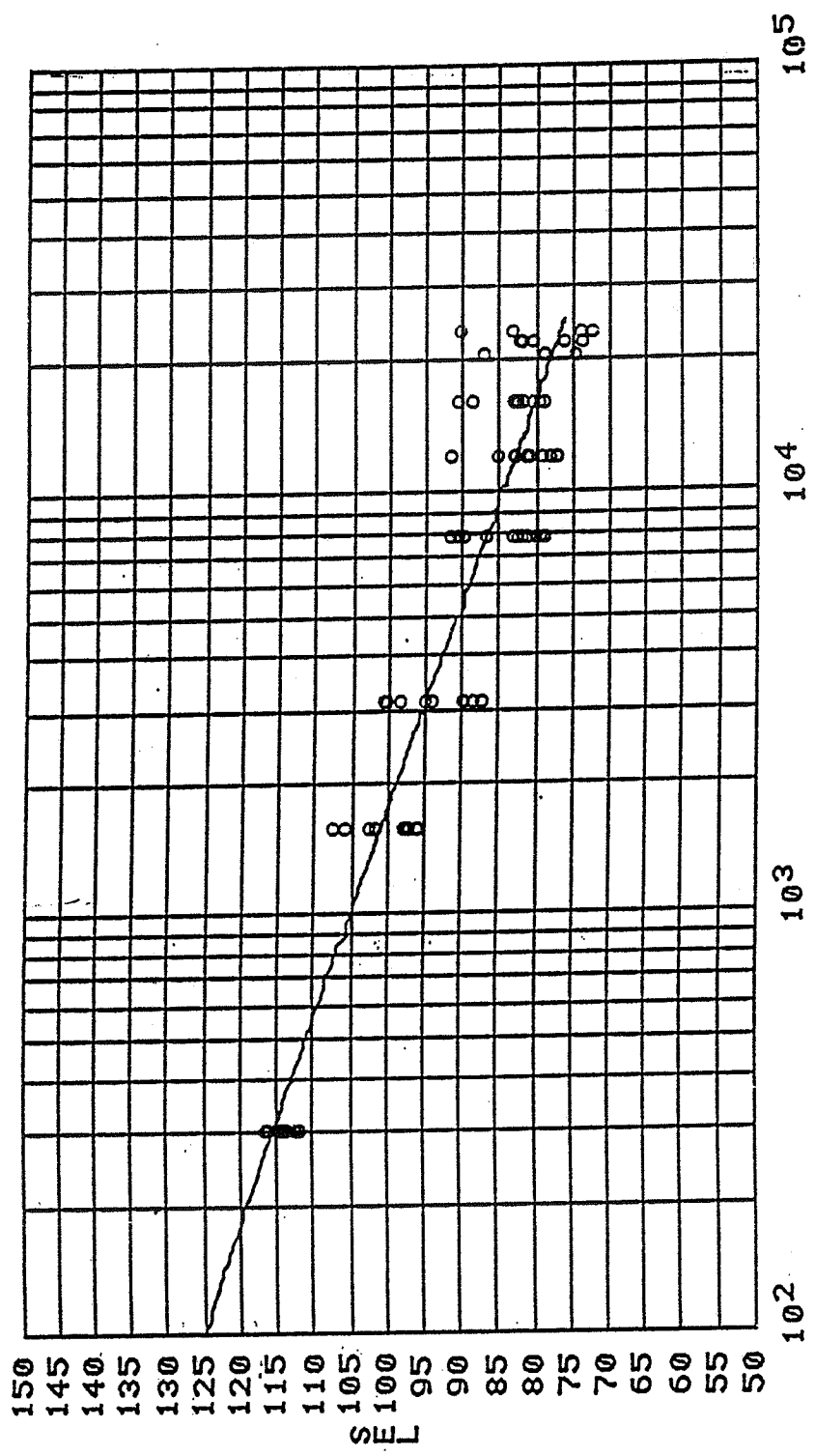

Figure 34. CSEL vs. distance for constant below lapse category data from Aberdeen Proving Ground and FFP output.

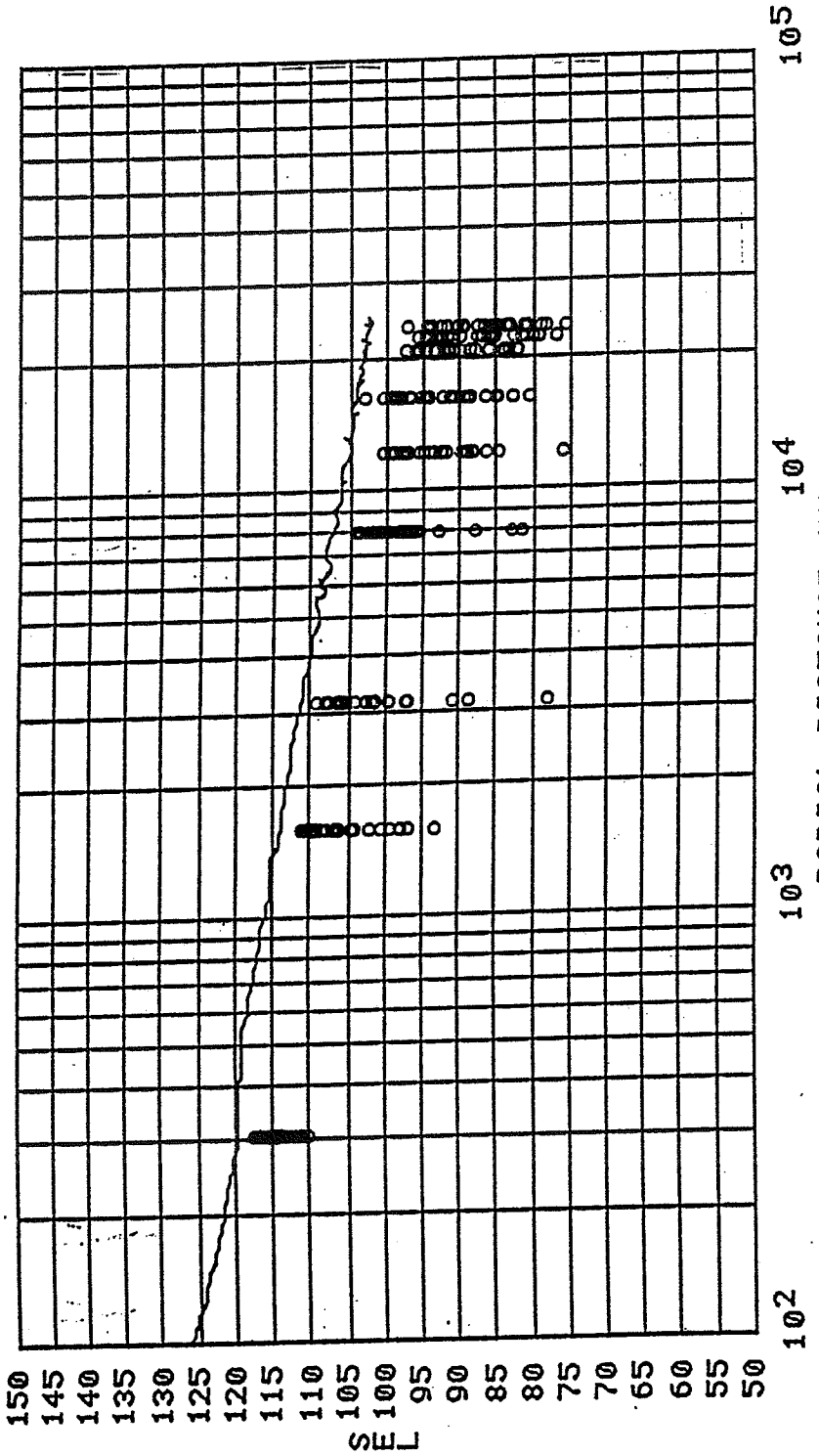

Figure 35. CSEL vs. distance for low inversion category data from Aberdeen Proving Ground and FFP output.

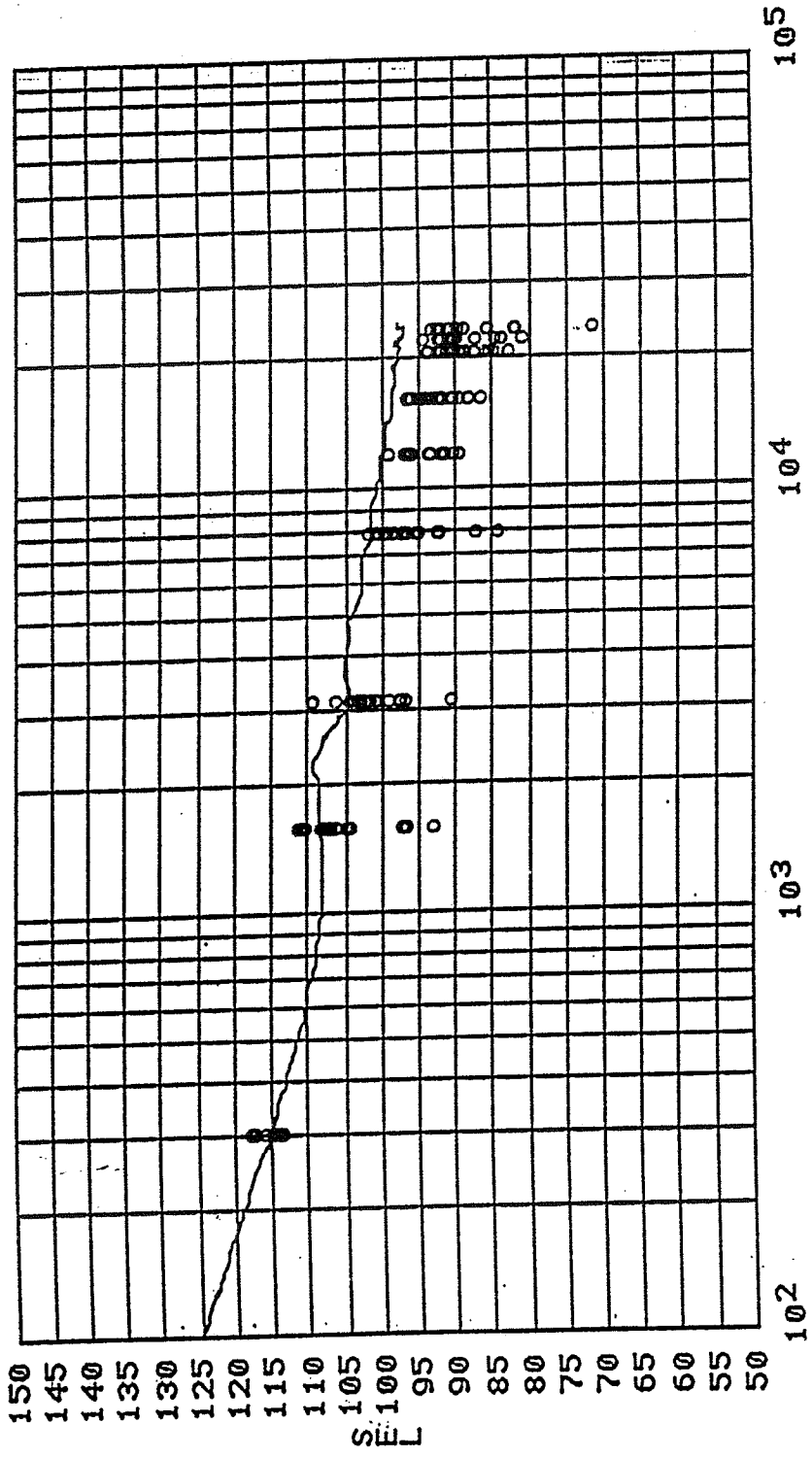

Figure 36. CSEL vs. distance for medium inversion category data from Aberdeen Proving Ground and FFP output.

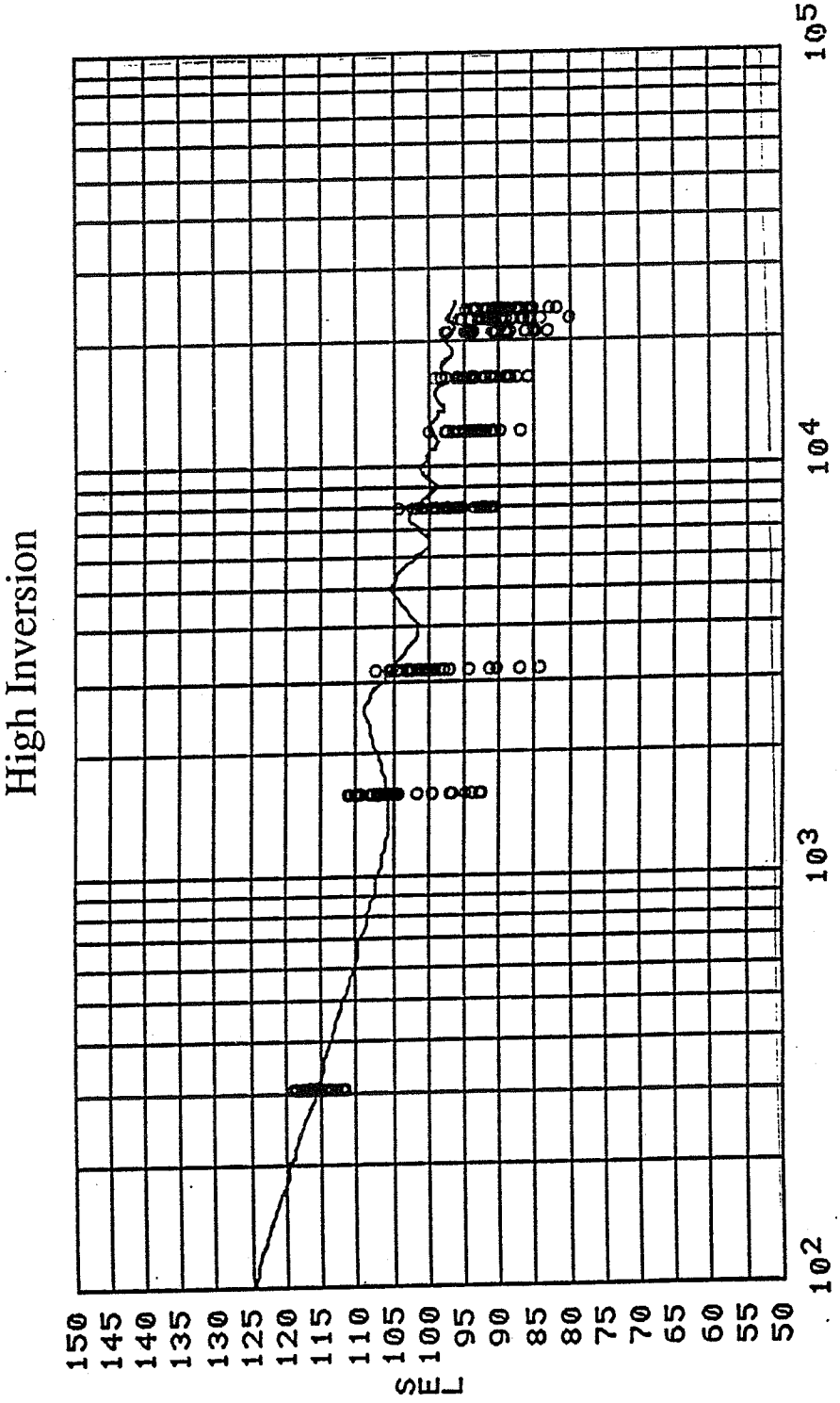

Figure 37. CSEL vs. distance for high inversion category data from Aberdeen Proving Ground and FFP output.

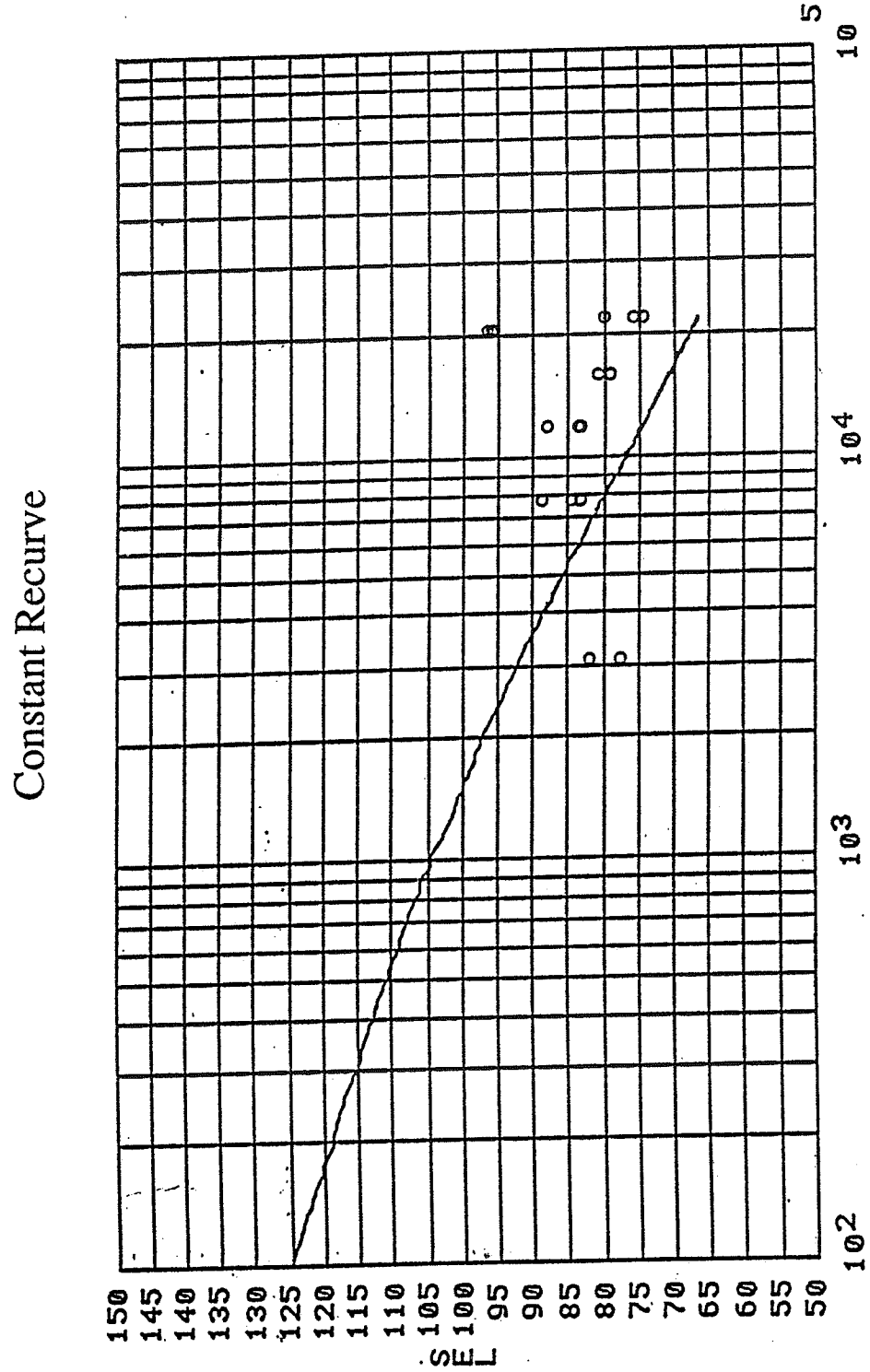

Figure 38. CSEL vs. distance for constant recurve category data from Aberdeen Proving Ground and FFP output.

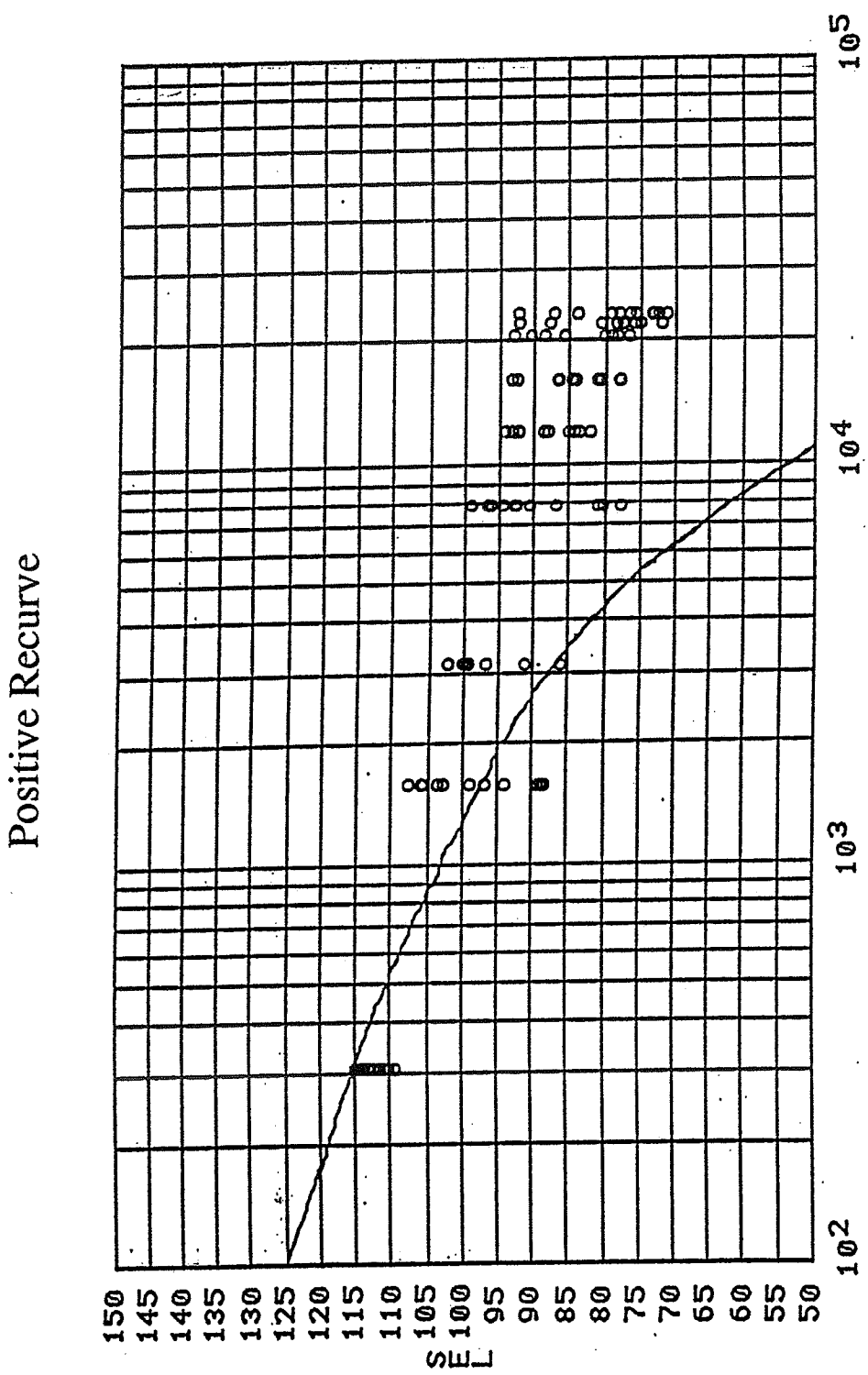

Figure 39. CSEL vs. distance for positive recurve category data from Aberdeen Proving Ground and FFP output.

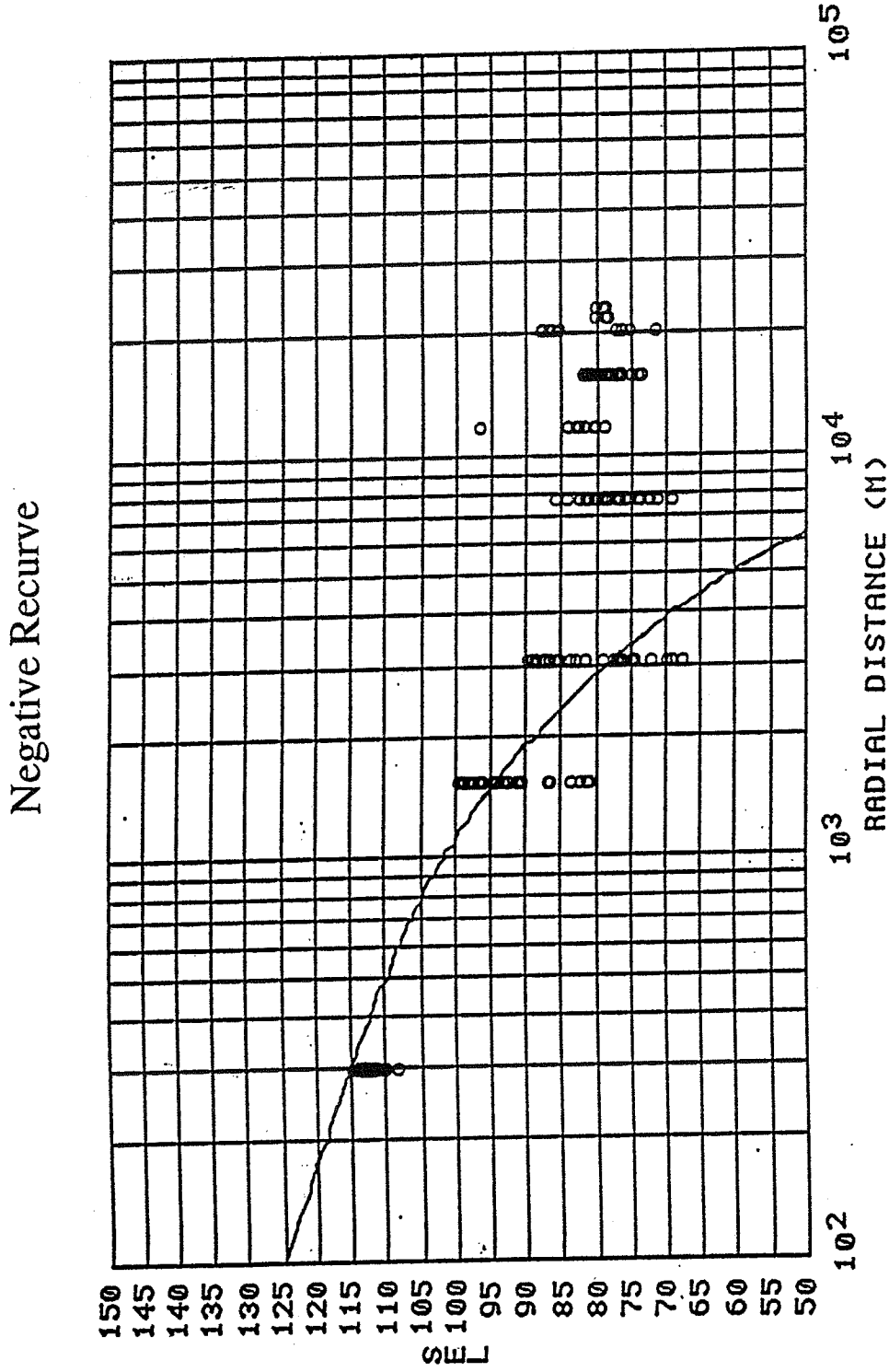

Figure 40. CSEL vs. distance for negative recurve category data from Aberdeen Proving Ground and FFP output.

VIII. CONCLUSIONS

This chapter presents several interesting things that can be gathered from studying the results presented in the previous chapter. The agreement of the data with the prediction is discussed as well as phenomena associated with blast propagation.

In general, for the Fort Bliss data, the FFP tends to overpredict sound exposure levels for the constant profile while severely underpredicting for upward refracting profiles. Agreement is good for downward refracting situations. For Aberdeen data, we see a good correspondence between the FFP result and the data for the constant profile. Overprediction is observed in the inversion cases, while extreme underprediction is noted for upward refracting cases. Conditions or assumptions affecting the accuracy of predictions are now considered.

A. Grouping

The first and most obvious question one might ask about the results is whether the data were grouped into the most appropriate category for the best correspondence with the prediction. This concern was investigated by regrouping the data and rerunning the FFP to check for any significant change. The first step toward this end led to grouping the downward refracting data sets (inversions) by the slope of the sound velocity profile rather than the height of the maximum sound speed. Unfortunately, of all the inversion cases few corresponded in slope.

Three new groupings were tried: two groups from Fort Bliss inversions and one from Aberdeen inversions. Each group contained only two or three sound velocity profiles similar in slope.

A linear equation was written to describe the increasing sound velocity with height. Using this equation, the sound velocity was calculated at the center of each layer to be run in the FFP. Once again, twelve layers were used. The output was then compared with the actual data.

The actual data were grouped much more tightly than the data that were not grouped by slope. Yet this is deceiving due to the small number of data sets in each group. The results showed no discernible difference between the predicted SEL values and the mean experimental values.

It should be noted here that the FFP layers extend up to 100 meters only and are capped with a homogeneous half-space. Through experimentation with varying thickness and numbers of layers, it was shown that structures in the sound velocity profile above 100 meters do not change the prediction of the FFP. At ranges greater than what we have considered and during different seasons this is not necessarily true. Consequently, the linear equation is simply a positively increasing sound velocity with height that describes the atmosphere in the lowest 100 meters.

The above implies yet another issue. Given that the sound velocity profile above 100 meters is immaterial, we may reduce the nine groups chosen to represent all sound velocity profiles. The first 100 meters of the constant, constant recurve and the constant below lapse are identical and can therefore be combined into one group. The same holds true for the negative recurve, positive recurve and lapse as well as the previously mentioned inversion groups. The similarity of the bottom 100 meters of the indicated profiles can be reviewed in Figure 6. One should also note the similarity of the SEL vs. range plots of the indicated groups in Figures 25-40.

B. Instability Over Range

Another way in which discrepancy may occur between data and prediction appears in the assumption that the sound velocity profile is uniform over the range. The FFP solution is dependent on this assumption. Unfortunately, this is not entirely true. Another method of prediction is currently being investigated in which this is not a problem. The solution of the parabolic equation may prove to be a more accurate prediction method in this respect [23].

C. Sensitivity to Flow Resistivity

In all cases at Ft. Bliss the flow resistivity was equal to 100 cgs Rayls. This parameter was not actually measured, but assumed because of the similarity of this surface to others in previous experiments. As seen in Figure 41, variation in the flow resistivity can be significant away from the source. For an inversion case, at ten kilometers, sound exposure levels between a surface with a flow resistivity of 50 and one with a flow resistivity of 200 cgs Rayls differ by 10 dB.

D. Surface Hardness

Having two different bottom surfaces in the two experiments conducted is useful for comparing similar categories with dissimilar grounds.

The most apparent difference between the SEL vs. range curves for the two surfaces in each category is the higher levels over water. This is not surprising since intuitively one would expect a larger reflected component from a harder surface.

In addition to the difference in pressure amplitude for the two surfaces, the way in which the amplitude falls off with distance is different for each case. As suggested in [24], for downward refracting profiles and high impedance ground (hard), it is observed that for low frequencies propagation is nearly cylindrical with a decay of $1/r^{-1/2}$. For lower impedance surfaces and higher frequencies, spherical spreading dominates in the first kilometer or so, turning briefly to cylindrical spreading and culminates in an exponential decay due to the absorptive nature of the soft surface. The progression for each case is observed in Figures 27-29 and Figures 35-37.

E. Turbulence

Turbulence can affect sound propagation in ways that are difficult to quantify. It is believed that turbulence scatters sound energy into shadow zones produced by upward refracting profiles. This phenomenon can be viewed in Figure 24 and Figure 32. In these figures, both for lapses, one can see that the FFP underpredicts the actual levels by as much as thirty-five dB at ten kilometers. Given that our experiments were performed in relatively unstable summer conditions, it appears that the lower atmosphere dominates the propagation. Turbulence seems to produce most of the effects observed. The FFP predicts such low SELs because the microphones, at long ranges, in the shadow zone, receive no direct rays. With the inclusion of turbulence into the FFP scheme, it is thought that agreement will improve. More information on turbulence can be found in [25].

F. Sound Velocity Profile Representation

The curved lines sketched in as average sound velocity profiles in Figures 7-23 were tested for their validity of being good representations of the actual curves. As can be noted, the actual curves are quite jagged while the average profile was depicted as being very smooth. In order to assess the results of this assumption, the most wildly varying sound velocity profile was chosen from the lapse category and also from the low inversion category from Ft. Bliss. The actual sound velocity data was entered for a 12 layer FFP run and compared against the FFP output produced by inserting the averaged curve. In both instances, there was no variation from the run with the averaged curve. Looking at the actual data curves only up to one hundred meters shows that variation of sound speed is rather smooth. This indicates that using an approximated curve, in the afore mentioned manner, is reasonable. For this reason, we can see that levels are not very sensitive to details of the profile.

G. Surface Roughness

Another concern in accurately predicting sound levels is the roughness of the bounding surface. The study of how irregularities of a surface, smaller than a wavelength, contribute to the alteration of the surface impedance and ultimately sound propagation is only recently being widely explored. Howe [26] shows that surface roughness can generate a surface wave that can penetrate into a shadow zone. This surface wave would be responsible for increasing levels. At this time it remains unclear as to the significance of the surface wave's contribution. Again, with the inclusion of a roughness parameter in the FFP, prediction will become more accurate.

H. Summary

As can be seen from the several topics previously discussed, the accurate prediction of pressure fields is not a trivial problem. Many factors must be taken into account. Although, the current FFP provides a good estimate, it is not perfect. Researching the above mentioned subjects and incorporating the results into the FFP will keep researchers busy for some time to come. Yet, with the stated shortcomings, the FFP remains one of the most advanced methods of blast noise

propagation prediction. We have an increased insight of the physical propagation of acoustic waves and a highly functional prediction model to look forward to as the FFP comes of age.

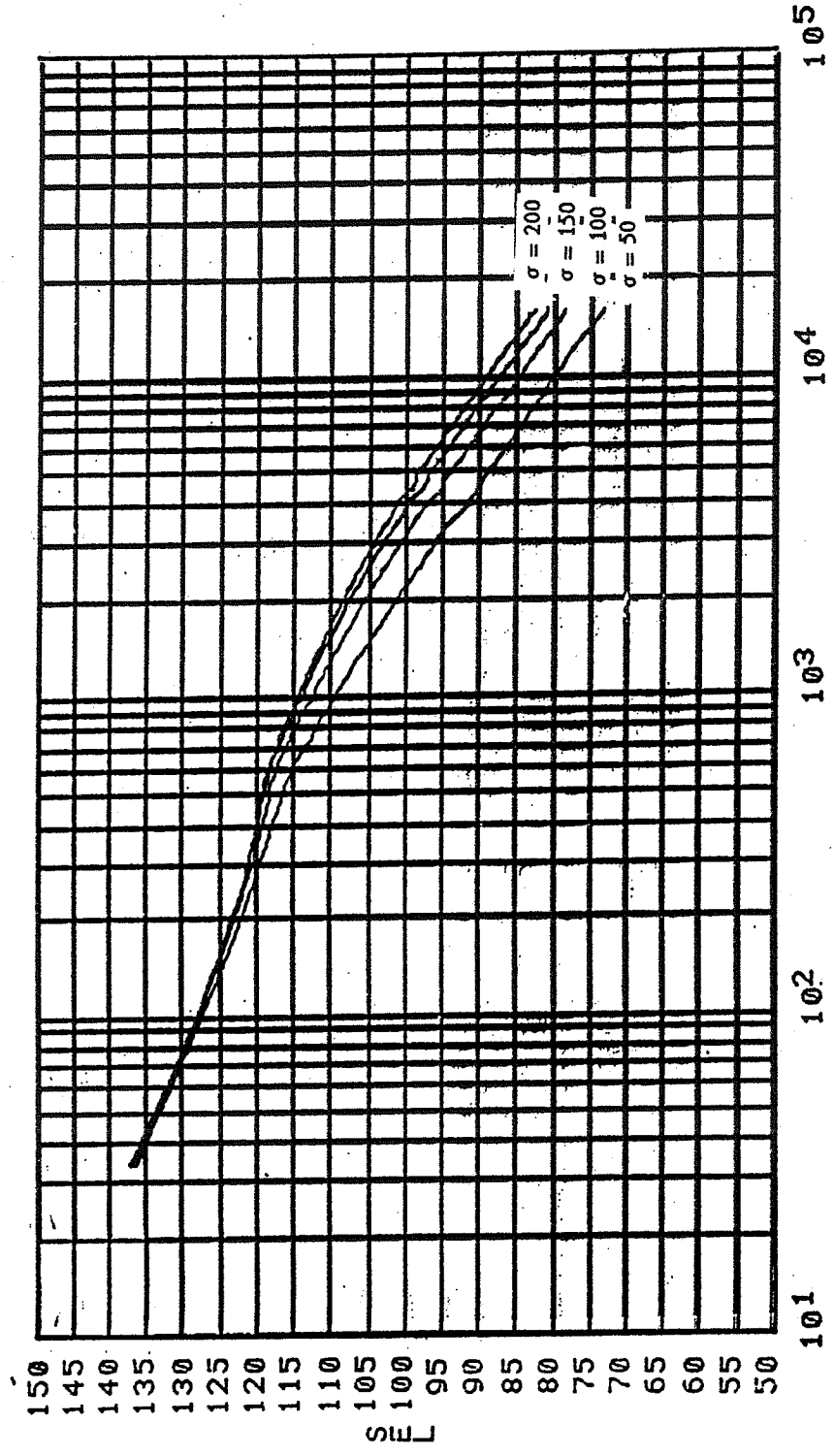

Figure 41. Variation in CSEL vs. distance due to change in flow resistivity.

REFERENCES

[1] E. H. Brown and F. F. Hall, Jr., "Atmospheric acoustics," Reviews of Geophysics and Space Physics **16**(1), pp. 47-110, 1978.

[2] U. Ingard, "A review of the influence of meteorological conditionson sound propagation," J. Acoust. Soc. Am. **25**(3), pp. 405-411, May 1953.

[3] E. F. Cox, H.J. Plagge and J.W. Reed, "Meteorology directs where blast will strike," B.Am. Meteor. Soc. **35**, pp. 95-103, 1954.

[4] W. J. Noble, "On the effects of reflection and refraction in a velocity gradient," J. Acoust. Soc. Am. **27**(5), pp. 888-891, September 1955.

[5] B. Perkins and W. F. Jackson, "Handbook for prediction of air blast focussing," Ballistic Research Laboratories, Report 1240, February 1964.

[6] J. W. Reed, "Acoustic wave effects project: Airblast prediction techniques," Sandia Laboratories, Report SC-M-69-332, May 1969.

[7] R. A. Rasmussen, "A prediction method for blast focussing," USAF Environmental Technical Applications Center, Tech. Rep. 71-8, September 1971.

[8] R. C. Bundgaard, "The effects of atmospheric fluctuations and representation upon propagated sound," NASA contractor report CR-1337, April 1969.

[9] P. Schomer, L. Little, D. L. Effland, V. I. Pawlowska, S. G. Roubik, "Data Bases and Computational Procedures: Vol. I-II," US Army Construction Engineering Research Laboratory, Rept. N-98.

[10] G. Kerry, D.J. Saunders and A. G. Sills, "The use of meteorological profiles to predict the peak sound-pressure level at distance from small explosions," J. Acoust. Soc. Am. **81**(4), pp. 888-896, April 1987.

[11] F. R. DiNapoli and R. L. Deavenport,"Theoretical and numerical Green's function field solution in a plane multilayered medium," J. Acoust. Soc. Am. **67**(1), pp. 92-105, January 1980.

[12] H. W. Kutschale, "Rapid computation by wave theory of the propagation loss in the Arctic Ocean," Tech. Rep. #8, Lamont-Doherty Geological Observatory, Columbia University, Palisades, NY, 1973.

[13] R. Raspet, S. W. Lee, E. Kuester, D.C. Chang, W. F. Richards, R. Gilbert, and N.Bong, "Fast-field program for a layered medium bounded by complex impedance surfaces," J. Acoust. Soc. Am. **77**, pp. 345-352, February 1985.

[14] S. W. Lee, N. Bong, W. F. Richards, and R. Raspet, "Impedance formulation of the fast field program for acoustic wave propagation in the atmosphere, " J.Acoust.Soc. Am.**79**, pp. 628-634, March 1986.

[15] A. D. Pierce, Acoustics an Introduction to Its Physical Principles and Applications . New York: McGraw-Hill, 1981, Chap. 8.

[16] R. B. Lindsay, Physical Acoustics. Stroudsburg, PN: Dowden, Hutchinson and Ross, Inc, 1974.

[17] R. Geiger, The Climate Near the Ground. Cambridge,MS: Harvard University Press, 1959.

[18] M. E. Delany and E.N. Bazley, "A note on the effect of ground absorption in the measurement of aircraft noise," J. Sound Vib. **16**(3), pp. 315-322, June 1971.

[19] C. I. Chessell, "Propagation of noise along a finite impedance boundary," J. Acoust. Soc. Am. **62**(4), pp. 825-834, October 1977.

[20] S. J. Franke, C. H. Liu and S. W. Lee, "Numerical computation of the acoustic transfer function and transient response," U.S. Army Construction Engineering Research Lab., Champaign, IL, Internal Report, 1985.

[21] A. Averbuch, "True-Integrating Environmental Noise Monitor and Sound Exposure Level Meter: Vol. I-IV," Tech. Rept. N-41, US Army Construction Engineering Research Laboratory,Champaign, IL, 1978.

[22] F. D. Shields and H. E. Bass, "Atmospheric absorption of high frequency noise and application to fractional-octave bands," NASA contractor report CR-2760, 1969.

[23] "NORDA Parabolic Equation Workshop," edited by J.A. Davis, D. White and R.C Cavanagh, Rept. TN-143, Naval Ocean Research and Development Activity, Bay St. Louis, MS, 1982.

[24] R. Raspet and R. Wolf, "Application of the FFP to Outdoor Sound Propagation," Proceedings of 1986 International Conference on Noise Control Engineering, Cambridge, MA, 1986.

[25] V. I. Tatarski, "The effects of the turbulent atmosphere on wave propagation," Tech. Rept. TT-68-50464, US Department of Commerce, National Technical Information Service, Springfield,VA, 1971.

[26] M. S. Howe, "On the long range propagation of sound over irregular terrain," J. Sound Vib. **98**(1), pp. 83-94, January 1985.